

Robust Energy System Design via Semi-infinite Programming

Moritz Wedemeyer^{a,b}, Eike Cramer^c, Alexander Mitsos^{d,a,c}, Manuel Dahmen^{a,*}

^a Institute of Climate and Energy Systems, Energy Systems Engineering (ICE-1), Forschungszentrum Jülich GmbH, Jülich 52425, Germany

^b RWTH Aachen University, Aachen 52062, Germany

^c RWTH Aachen University, Process Systems Engineering (AVT.SVT), Aachen 52074, Germany

^d JARA-ENERGY, Jülich 52425, Germany

Time-series information needs to be incorporated into energy system optimization to account for the uncertainty of renewable energy sources. Typically, time-series aggregation methods are used to reduce historical data to a few representative scenarios but they may neglect extreme scenarios, which disproportionately drive the costs in energy system design. We propose the robust energy system design (RES-D) approach based on semi-infinite programming and use an adaptive discretization-based algorithm to identify worst-case scenarios during optimization. The RES-D approach can guarantee robust designs for problems with nonconvex operational behavior, which current methods cannot achieve. The RES-D approach is demonstrated by designing an energy supply system for the island of La Palma. To improve computational performance, principal component analysis is used to reduce the dimensionality of the uncertainty space. The robustness and costs of the approximated problem with significantly reduced dimensionality approximate the full-dimensional solution closely. Even with strong dimensionality reduction, the RES-D approach is computationally intense and thus limited to small problems.

Keywords: *Semi-infinite programming, Robust optimization, Energy system design, Variable renewable energy sources*

*M. Dahmen, Institute of Climate and Energy Systems, Energy Systems Engineering (ICE-1), Forschungszentrum Jülich GmbH, Jülich 52425, Germany
E-mail: m.dahmen@fz-juelich.de

1 Introduction

The transformation of energy supply systems from fossil energy sources to variable renewable energy resources (VRES) has increased the volatility of electricity supply and, consequently, demand. This volatility introduced by the stochastic nature of VRES has led to new challenges in the design and operation of energy systems (Gross et al., 2007; Huber et al., 2014; Heptonstall and Gross, 2021).

Mathematical optimization is an effective tool to design energy systems that are optimal, e.g., have minimal total annualized cost or global warming impact, and can be leveraged to design energy systems that are robust towards the volatility introduced by VRES (Biegler and Grossmann, 2004; Yunt et al., 2008; Lubin et al., 2011; Li and Barton, 2015). Optimization has been successfully applied to design energy systems across various scales, from utility systems at the plant scale (Papoulias and Grossmann, 1983; Voll et al., 2013; Bahl et al., 2018; Baumgärtner et al., 2019) to energy systems for districts (Bünning et al., 2018; Schütz et al., 2018; Teichgraeber and Brandt, 2019) up to power systems on islands (Ma et al., 2014; Gils and Simon, 2017; Barone et al., 2021) and on the (inter)-national scale (Kannan and Turton, 2013; Siala et al., 2019; Reinert et al., 2020). For a review of modeling tools for renewable energy systems, we refer to Ringkjøb et al. (2018).

Modeling the volatility of VRES leads to uncertainties in the optimization problem parameters. Two popular approaches to account for uncertain parameters are stochastic programming (Dantzig, 1955) and robust optimization (Campo and Morari, 1987). Stochastic programming requires knowledge of the probability distribution of the uncertain parameters and optimizes the expected value of the objective function. Robust optimization, on the other hand, guarantees the feasibility of an optimal solution for all parameters within a predefined uncertainty set and does not require the probability distribution. For detailed information on stochastic programming and robust optimization, we refer to Birge and Louveaux (2011) and Ben-Tal et al. (2009), respectively.

To capture the time-varying behavior of VRES, the probability distribution can be approximated discretely by including historical time-series data in the optimization as scenarios in a two-stage stochastic programming (Dantzig, 1955) formulation of the design problem (Teichgraeber and Brandt, 2022). A sufficiently high temporal resolution is needed to properly account for the time-varying behavior of renewable electricity production (Poncelet et al., 2016; Keles et al., 2017; Ringkjøb et al., 2018). Excessive use of historical data and high temporal resolutions, however, increase the number of constraints and variables of the optimization problem, thus leading to computationally intractable formulations (Pfenninger et al., 2014; Hoffmann et al., 2020). Therefore, tradeoffs between computational tractability and the degree of detail in which the system is modeled are necessary.

Different dimensions of model complexity reduction can be leveraged to facilitate computational tractability. First, model complexity can be reduced by spatial aggregation. A prominent and extreme example is the copper plate assumption, where the spatial distribution is completely ignored, and transmission losses are neglected (Hess et al., 2018). Furthermore, temporal model complexity can be reduced by using only a representative subset of the historical time-series data, e.g., a collection of representative days (Chapaloglou et al., 2022). A popular method to determine representative scenarios is clustering (Kotzur et al., 2018; Teichgraeber and Brandt, 2019). However, aggregation methods may neglect extreme scenarios, which may impact the operational feasibility of the optimal system design.

Heuristic methods have been introduced to incorporate extreme scenarios during the design. The heuristics identify and add extreme scenarios to the optimization problem before performing the design optimization. For example, Domínguez-Muñoz et al. (2011) exclude days with peak demands from the aggregation and add these to the scenario data of the problem directly. However, by incorporating individual peak days for the different energy demand forms, e.g., heat, cooling, and electricity, interactions between these demand forms may get lost. Furthermore, when multiple uncertain quantities are considered, e.g., solar electricity production and electricity demand, the worst-case realization might not correspond to scenarios where the quantities are at their extreme values but rather a scenario where the interaction of their values creates the largest supply and demand mismatch.

Furthermore, the worst-case scenario depends on the energy system design; for example, the installed capacities of solar PV and wind turbines in an energy system influence whether scenarios with low wind speeds or low solar irradiance are critical. *A priori* extreme period selection cannot consider this influence of the design on the extreme periods.

To mitigate this problem, extreme periods specific to a given (preliminary) design can be identified by optimizing the system *operation*, i.e., by determining whether the considered design can satisfy energy demands for all historical scenarios. Scenarios in which operations are found to be infeasible are then added as extreme periods to the design problem formulation, and subsequently, another design optimization is performed. In the context of energy system design, Bahl et al. (2016) introduced such an iterative heuristic in which they repeatedly solve a design problem with approximated operational costs and add virtual time steps for which the operational problem becomes infeasible until eventually a design is obtained that can supply all historical scenarios. The solution approach that Bahl et al. (2016) use to identify worst-case scenarios from a set of finite cardinality is very similar to the algorithm proposed by Blankenship and Falk (1976) to solve semi-infinite programs (SIPs). Teichgraeber et al. (2020) developed this concept further and referred to it as the optimization-based feasibility time-step heuristic.

We will refer to this approach as the *feasibility time-step heuristic* for brevity. However, as we will show, considering only the historical data may not be enough to identify robust designs. Specifically, if the operational problem is nonconvex, the identified system design may not be feasible for scenarios that lie “between” historical scenarios, i.e., that constitute convex combinations of historical data.

Addressing the aforementioned challenges, we propose a rigorous and robust energy system design (RESD) approach that identifies worst-case scenarios from a predefined space of possible uncertainty realizations *during* the optimization. The RESD approach bears similarity to the approach for optimal process design under uncertainty by [Halemane and Grossmann \(1983\)](#). We formulate the energy system design problem as a two-stage stochastic program, where we approximate the objective by discretization but treat the constraints continuously by formulating them as semi-infinite constraints ([Charnes et al., 1962](#); [Grossmann and Sargent, 1978](#); [Hettich and Kortanek, 1993](#); [Djelassi et al., 2021](#)). The discretized approximation of the objective is obtained by approximating the operational costs using a small number of representative scenarios that we determine using clustering. To address the neglect of extreme scenarios by clustering, the semi-infinite constraints enforce feasible operation for all scenarios within a predefined uncertainty space and guarantee the robustness of the identified design towards the volatility introduced by the VRES and the energy demand. Semi-infinite programs often arise in robust design problems ([Ben-Tal and Nemirovski, 2002](#)); for reviews of semi-infinite programming, we refer to [Hettich and Kortanek \(1993\)](#); [Rückmann and Reemtsen \(1998\)](#); [Guerra Vázquez et al. \(2008\)](#); [Stein \(2012\)](#).

The key difference between established methods in energy system design, such as the feasibility time-step heuristic, and the RESD approach is the ability of the latter to consider continuous uncertainty spaces, i.e., allow the sets of possible uncertainty realizations to have infinite cardinality. In contrast, the feasibility time-step heuristic is constrained to finite cardinality sets. The space of uncertainty realizations can be defined arbitrarily; a straightforward example of such a set is a box-constrained set. In the present work, we define the uncertainty space by means of the convex hull around the historical data, i.e., we consider convex combinations of historical data as possible uncertainty realizations.

The optimization problem corresponding to the RESD approach is a three-level hierarchical program that is computationally challenging to solve. If all historical data points are contained within the bounded part of the search space, the optimization problem corresponding to the RESD approach is a restriction of the problem considered in the feasibility time-step heuristic ([Bahl et al., 2016](#); [Teichgraeber et al., 2020](#)). A solution to the restricted problem is robust for more scenarios than the original problem but may have a worse objective function value.

In previous work, we demonstrated that principal component analysis (PCA) is well suited to re-

duce the dimensionality of energy time-series data (Cramer et al., 2022). To facilitate computational tractability, we use PCA (Pearson, 1901) to reduce the dimensionality of the data in the RESD approach. Furthermore, we utilize a lifting approach to improve computational tractability for design problems where the problem of determining the optimal operational strategy is convex. Specifically, we leverage that the lower-level problem is a convex optimization problem to reformulate the problem as a SIP using the approach proposed by Diehl et al. (2013).

The remainder of this work is structured as follows: Section 2 introduces the problem structure associated with the RESD approach and explains how the historical data is incorporated into the optimization problem. In Section 3, we use an illustrative mixed-integer linear problem (MILP) example to demonstrate the shortcomings of the feasibility time-step heuristic in identifying relevant extreme scenarios and demonstrate the robustness of the RESD approach. Furthermore, special cases in which the feasibility time-step heuristic (Bahl et al., 2016; Teichgraber et al., 2020) yields identical results to the RESD approach are pointed out. Finally, the lifting approach based on Diehl et al. (2013) is introduced to improve computational performance for problems with convex operational behavior. By means of a case study on the La Palma energy system, Section 4 then analyzes the accuracy of the designs obtained by the RESD approach and the influences of the dimensionality reduction and the lifting approach on the computational performance. Finally, Section 5 summarizes our work.

2 Robust Energy System Design Approach

Robust energy system designs are feasible for all considered uncertainty realizations, i.e., they are able to supply the energy demand while satisfying all operational constraints. However, they are not robust with respect to the objective, i.e., they do not give a guaranteed bound on the operational costs. The RESD approach relies on two concepts to identify robust designs that are cost-optimal: (i) the operational costs are estimated using a small number of representative scenarios with associated probabilities of occurrence (Chapaloglou et al., 2022), (ii) an embedded optimization problem ensures the feasibility for all possible uncertainty realizations within a predefined uncertainty set.

$$\begin{aligned}
& \min_{\mathbf{x}, \mathbf{z}_s} \quad \text{Investment costs}(\mathbf{x}) + \sum_{s \in \mathcal{S}} \text{Operational costs}(\mathbf{z}_s), & (\text{PS}) \\
& \text{s.t.} \quad \mathbf{g}_{en}(\mathbf{x}, \mathbf{y}_s, \mathbf{z}_s) \leq \mathbf{0} \quad \forall s \in \mathcal{S} \quad (\text{Energy system model}), \\
& \quad \maxmin_{\mathbf{y} \quad \mathbf{z}} \quad \text{Energy gap}(\mathbf{x}, \mathbf{y}, \mathbf{z}) \leq 0, \\
& \text{s.t.} \quad \mathbf{g}_{en}(\mathbf{x}, \mathbf{y}, \mathbf{z}) \leq \mathbf{0} \quad (\text{Energy system model}), \\
& \quad \mathbf{g}_y(\mathbf{y}) \leq \mathbf{0} \quad (\text{Uncertainty bounds}),
\end{aligned}$$

(PS) shows the general structure of the RESD problem. The upper-level problem is the deterministic equivalent of a two-stage stochastic program (Birge and Louveaux, 2011) with a discrete approximation of the scenarios by fixed uncertainty realizations \mathbf{y}_s and determines the optimal design decisions \mathbf{x} , such as the installed capacities of renewable generators, to achieve a cost-optimal design with respect to the expected value of the operational costs, which is calculated by estimating operational costs with operational decisions \mathbf{z}_s . While we assume that the investment costs are not subject to uncertainty, the operational costs depend on future uncertainty realizations, e.g., on the solar irradiance; thus, we estimate their expected value by means of representative scenarios \mathcal{S} (Chapaloglou et al., 2022).

Furthermore, $\mathbf{g}_{en}(\cdot, \cdot, \cdot)$ are the constraints modeling the energy system, which occur both in the upper- and lower-level problem to ensure the feasibility of the operational decisions associated with the representative scenarios and the extreme scenarios.

$$\begin{aligned}
& \maxmin_{\mathbf{y} \quad \mathbf{z}} \quad \text{Energy gap}(\mathbf{x}, \mathbf{y}, \mathbf{z}) \leq 0, & (\text{MLP}) \\
& \text{s.t.} \quad \mathbf{g}_{en}(\mathbf{x}, \mathbf{y}, \mathbf{z}) \leq \mathbf{0} \quad (\text{Energy system model}), \\
& \quad \mathbf{g}_y(\mathbf{y}) \leq \mathbf{0} \quad (\text{Uncertainty bounds}),
\end{aligned}$$

To ensure robustness, an embedded optimization problem, which we refer to as the medial-level problem (MLP), guarantees that the energy supply gap is nonpositive for all possible uncertainty realizations \mathbf{y} , i.e., the energy supply meets or exceeds the energy demand. This is achieved by identifying the worst-case uncertainty realization for the superordinate design within the predefined uncertainty set defined by $\mathbf{g}_y(\mathbf{y}) \leq \mathbf{0}$. Reaction to the uncertainty realizations, i.e., recourse actions (Birge and Louveaux, 2011), is considered through operational decisions \mathbf{z} , e.g., battery charge and discharge decisions.

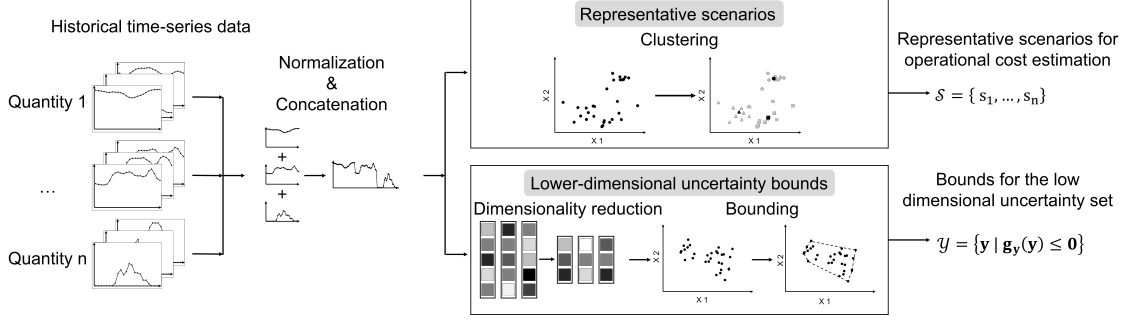


Fig. 1. The processing of historical time-series data to obtain the representative scenarios and uncertainty bounds for the RESD problem: Time-series data with the length of the representative period are collected for different quantities, normalized, and concatenated such that a single vector is obtained for each representative period in the historical data. Representative scenarios are obtained by clustering the concatenated and normalized data according to the framework by [Teichgraeber and Brandt \(2019\)](#). Uncertainty bounds are obtained by first reducing the dimensionality of the historical data and then determining bounds in the lower-dimensional space.

2.1 Processing of Historical Data

The RESD approach requires representative scenarios for operational cost estimation and uncertainty bounds that delimit the search space for the identification of worst-case uncertainty realizations. We choose to obtain both from historical time-series data. Figure 1 shows the corresponding data processing step. For each quantity of interest, e.g., solar irradiance, the historical time-series data is split into the desired representative period length, e.g., a representative day.

First, representative scenarios are chosen according to the framework by [Teichgraeber and Brandt \(2019\)](#), where normalization helps to ensure equal weighting of different quantities during clustering. The normalized time-series data for each attribute, e.g., solar irradiance and electricity demand, are then concatenated, and representative scenarios are selected by clustering. Clustering on the concatenated quantities is necessary to maintain the temporal coherence between different quantities. The choice of the employed normalization technique, clustering method, and parameters is generally problem-specific; we refer to [Teichgraeber and Brandt \(2019\)](#) for guidance.

Second, the bounds for the uncertainty set need to be determined. In previous work, we showed that time-series scenarios for renewable energy sources lie on linear lower-dimensional manifolds ([Cramer et al., 2022](#)). Accordingly, we introduce a dimensionality reduction step to facilitate better computational tractability of the RESD problem. The dimensionality reduction shifts the worst-case search to a lower-dimensional latent space, reducing the number of variables in the embedded optimization problem. We choose principal component analysis (PCA) ([Pearson, 1901](#)) as a linear dimensionality reduction technique. In principle, nonlinear dimensionality reduction methods could be used. However, the cor-

responding reverse transformation is embedded in the optimization problem. Hence, using a nonlinear reverse transformation gives rise to a nonlinear and, thus, typically much more challenging optimization problem. Depending on the truncation error, the identified extreme scenarios can be more or less extreme in the original space, meaning that the identified designs could be over- or under-conservative.

After reducing the dimensionality of the historical data by a transformation into the principal component space, we need to determine bounds on the lower-dimensional uncertainty realizations. The use of nonlinear bounding techniques would give rise to nonlinear optimization problems. Instead, we choose the convex hull to bound the uncertainty realizations using linear equations. The convex hull can be defined as a convex combination of its vertices or as points that lie inside the combination of half-spaces, i.e., the faces of the convex hull (Avis et al., 1997); we refer to Section 2.2 of the supplementary material for more detailed information. Determining the convex hull has exponential time complexity with respect to the dimensionality of the data (Chazelle, 1993), so that for a larger number of principal components the time to compute the convex hull can become a bottleneck, even in comparison to the optimization runtime.

2.2 The RESD Approach Problem Formulation

In the following, constraints are hidden in the sets from which the optimization variables can be chosen for better readability. The (RESD) problem has the following form:

$$\begin{aligned} \min_{\mathbf{x} \in \mathcal{X}, \mathbf{z}_s \in \mathcal{Z}_s(\mathbf{x}, \mathbf{y}_s)} \quad & f(\mathbf{x}) + \sum_{s \in \mathcal{S}} f_o(\mathbf{z}_s), \\ \text{s.t.} \quad & \max_{\mathbf{y} \in \mathcal{Y}(\mathbf{x})} \min_{\mathbf{z} \in \mathcal{Z}(\mathbf{x}, \mathbf{y})} \max_{t \in \mathcal{T}} e_t(\mathbf{x}, \mathbf{y}, \mathbf{z}) \leq 0 \end{aligned} \tag{RESD}$$

(RESD) is a variant of the problem proposed by Halemane and Grossmann (1983) for optimal process design under uncertainty. It includes a cost function that depends on both design costs $f(\mathbf{x})$ and approximated operational costs $\sum_{s \in \mathcal{S}} f_o(\mathbf{z}_s)$. Furthermore, a constraint enforces feasibility in the worst-case: $\max_{\mathbf{y} \in \mathcal{Y}(\mathbf{x})} \min_{\mathbf{z} \in \mathcal{Z}(\mathbf{x}, \mathbf{y})} \max_{t \in \mathcal{T}} e_t(\mathbf{x}, \mathbf{y}, \mathbf{z}) \leq 0$. Here, \mathbf{x} are the design decision variables, e.g., installed PV capacity, and \mathbf{z}_s are the operational decision variables, e.g., battery charging or discharging rates. The subscript s is a scenario index and indicates that \mathbf{z}_s are the operational decisions associated with the respective scenario, while the fixed parameters \mathbf{y}_s are the uncertainty realizations for scenario s .

The robustness of the design is enforced by an embedded optimization problem, which requires that the energy supply gap $e_t(\mathbf{x}, \mathbf{y}, \mathbf{z})$, i.e., the difference between demand and supply of some energy form, e.g., electricity, has to be nonpositive, i.e., the supply must be equal to or exceed the demand, at all time

steps t in the set of considered time steps \mathcal{T} . In the case of multiple demands, e.g., electricity and heat ($n = 2$), $e_t(\mathbf{x}, \mathbf{y}, \mathbf{z})$ will be of the form

$$e_t(\mathbf{x}, \mathbf{y}, \mathbf{z}) = \max(e_{t,1}(\mathbf{x}, \mathbf{y}, \mathbf{z}), \dots, e_{t,n}(\mathbf{x}, \mathbf{y}, \mathbf{z})),$$

with n referring to the number of energy forms considered. The inequality constraint requiring the energy supply gap to be nonpositive has to hold for all possible uncertainty realizations \mathbf{y} , e.g., capacity factors for PV, while the operational variables \mathbf{z} can be adjusted to help meet the demand.

The set $\mathcal{X} = \{\mathbf{x} \in \mathbb{R}^{n_x} \mid \mathbf{h}_x(\mathbf{x}) = \mathbf{0}, \mathbf{g}_x(\mathbf{x}) \leq \mathbf{0}\}$ contains all feasible realizations of the design decisions and the set $\mathcal{Y}(\mathbf{x}) = \{\mathbf{y} \in \mathbb{R}^{n_y} \mid \mathbf{h}_y(\mathbf{x}, \mathbf{y}) = \mathbf{0}, \mathbf{g}_y(\mathbf{x}, \mathbf{y}) \leq \mathbf{0}\}$ describes the feasible set of the uncertainty realizations. Sets $\mathcal{Z}_s(\mathbf{x}) = \{\mathbf{z}_s \in \mathbb{R}^{n_{z_s}} \mid \mathbf{h}_{z_s}(\mathbf{x}, \mathbf{y}_s, \mathbf{z}_s) = \mathbf{0}, \mathbf{g}_{z_s}(\mathbf{x}, \mathbf{y}_s, \mathbf{z}_s) \leq \mathbf{0}\}$ and $\mathcal{Z}(\mathbf{x}, \mathbf{y}) = \{\mathbf{z} \in \mathbb{R}^{n_z} \mid \mathbf{h}_z(\mathbf{x}, \mathbf{y}, \mathbf{z}) = \mathbf{0}, \mathbf{g}_z(\mathbf{x}, \mathbf{y}, \mathbf{z}) \leq \mathbf{0}\}$ describe feasible operational states and are bounded by equations describing the technical behavior of the system, e.g., equations describing the charging and discharging capabilities of the battery, which additionally depend on the capacities of the installed components \mathbf{x} . The dimensions of the vectors are denoted by n_x, n_{z_s}, n_y, n_z , respectively.

The embedded optimization problem in (RES_D) can be replaced by a semi-infinite existence constraint (Djelassi, 2020):

$$\max_{\mathbf{y} \in \mathcal{Y}(\mathbf{x})} \min_{\mathbf{z} \in \mathcal{Z}(\mathbf{x}, \mathbf{y})} \max_{t \in \mathcal{T}} e_t(\mathbf{x}, \mathbf{y}, \mathbf{z}) \leq 0 \iff \forall \mathbf{y} \in \mathcal{Y}(\mathbf{x}) [\exists \mathbf{z} \in \mathcal{Z}(\mathbf{x}, \mathbf{y}) : \max_{t \in \mathcal{T}} e_t(\mathbf{x}, \mathbf{y}, \mathbf{z}) \leq 0]$$

If coupling inequality constraints, i.e., constraints of the form $\mathbf{g}_y(\mathbf{x}, \mathbf{y}) \leq \mathbf{0}$ that involve the design decisions \mathbf{x} and the uncertainty realizations \mathbf{y} , are present, the resulting problem is an existence-constrained generalized semi-infinite program (EGSIP) which can be solved by solving its existence-constrained semi-infinite program (ESIP) relaxation under some mild assumptions (Mitsos and Tsoukalas, 2015).

Note that special care must be taken if coupling equality constraints are present. In the medial-level problem, coupling equality constraints can contain both upper- and medial-level variables: $\mathbf{h}_y(\mathbf{x}, \mathbf{y}) = \mathbf{0}$. In the lower-level problem, coupling equality constraints can contain upper- and/or medial-level and lower-level variables: $\mathbf{h}_z(\mathbf{x}, \mathbf{y}, \mathbf{z}) = \mathbf{0}$. Problems with coupling equality constraints may require specialized algorithms since the convergence of the algorithms employed in this work is no longer guaranteed. However, the coupling equality constraints can be eliminated if they can be rearranged as explicit functions that define some dependent optimization variables as a function of the remaining (independent) variables. For example, consider a medial-level problem with coupling constraints $\mathbf{h}_y(\mathbf{x}, \mathbf{y}) = \mathbf{0}$. If the uncertainty realizations \mathbf{y} can be split into a dependent part $\tilde{\mathbf{y}}$ and an independent part $\bar{\mathbf{y}}$ and the coupling

equality constraints $\mathbf{h}_y(\mathbf{x}, \mathbf{y}) = \mathbf{h}_y(\mathbf{x}, \tilde{\mathbf{y}}, \bar{\mathbf{y}}) = \mathbf{0}$ can be rearranged into an explicit equation $\tilde{\mathbf{y}} = \tilde{\mathbf{y}}(\mathbf{x}, \bar{\mathbf{y}})$, $\tilde{\mathbf{y}}$ can be replaced by $\tilde{\mathbf{y}}(\mathbf{x}, \bar{\mathbf{y}})$ everywhere, thus eliminating the dependent variables and removing the coupling equality constraints. [Halemane and Grossmann \(1983\)](#) use this technique to replace the state variables in the operational stage by a function of the design variables, uncertainties, and operational variables. In the case that the coupling constraints cannot be rearranged as an explicit function, methods for solving SIPs containing implicit functions, such as the specialized algorithms proposed by [Djelassi et al. \(2019\)](#) and [Stuber and Barton \(2015\)](#) may be used.

To solve the (RES_D) problem, we first reformulate it as an EGSIP and then form the ESIP relaxation, which we solve using the algorithm introduced by [Djelassi and Mitsos \(2021\)](#) and implemented in the libDIPS software package ([Zingler et al., 2023](#)). To this end, we transform the embedded optimization problem, i.e., the $\max_{\mathbf{y} \in \mathcal{Y}(\mathbf{x})} \min_{\mathbf{z} \in \mathcal{Z}(\mathbf{x}, \mathbf{y})} \max_{t \in \mathcal{T}} e_t(\mathbf{x}, \mathbf{y}, \mathbf{z})$ problem, into a bi-level problem by introducing an auxiliary variable e_{epi} to the minimization problem, which moves the innermost maximization problem into the constraints of the superordinate minimization problem. Since \mathcal{T} is a finite set, we replace $\max_{t \in \mathcal{T}} e_t(\mathbf{x}, \mathbf{y}, \mathbf{z}) - e_{epi} \leq 0$ by one equation for each time step t and obtain the bi-level problem:

$$\begin{aligned} & \max_{\mathbf{y} \in \mathcal{Y}(\mathbf{x})} \min_{\mathbf{z} \in \mathcal{Z}(\mathbf{x}, \mathbf{y}), e_{epi}} e_{epi}, \\ \text{s.t.} \quad & e_t(\mathbf{x}, \mathbf{y}, \mathbf{z}) - e_{epi} \leq 0 \quad \forall t \in \mathcal{T} \end{aligned}$$

By including the auxiliary variable e_{epi} and the corresponding constraints in the set of lower-level variables $\mathcal{Z}_{epi}(\mathbf{x}, \mathbf{y}) = \{\mathbf{z} \in \mathbb{R}^{n_z}, e_{epi} \in \mathbb{R} \mid \mathbf{h}_z(\mathbf{x}, \mathbf{y}, \mathbf{z}) = \mathbf{0} \wedge \mathbf{g}_z(\mathbf{x}, \mathbf{y}, \mathbf{z}) \leq \mathbf{0} \wedge e_t(\mathbf{x}, \mathbf{y}, \mathbf{z}) - e_{epi} \leq 0 \quad \forall t \in \mathcal{T}\}$, we can write the embedded optimization problem as $\max_{\mathbf{y} \in \mathcal{Y}(\mathbf{x})} \min_{\mathbf{z} \in \mathcal{Z}_{epi}(\mathbf{x}, \mathbf{y})} e_{epi}$, and thus obtain for the full design problem:

$$\begin{aligned} & \min_{\mathbf{x} \in \mathcal{X}, \mathbf{z}_s \in \mathcal{Z}_s(\mathbf{x}, \mathbf{y}_s)} f(\mathbf{x}) + \sum_{s \in \mathcal{S}} f_o(\mathbf{z}_s), \\ \text{s.t.} \quad & \max_{\mathbf{y} \in \mathcal{Y}(\mathbf{x})} \min_{\mathbf{z} \in \mathcal{Z}_{epi}(\mathbf{x}, \mathbf{y})} e_{epi} \leq 0 \end{aligned}$$

This problem can now be reformulated as an EGSIP ([Djelassi and Mitsos, 2021](#)):

$$\begin{aligned} & \min_{\mathbf{x} \in \mathcal{X}, \mathbf{z}_s \in \mathcal{Z}_s(\mathbf{x}, \mathbf{y}_s)} f(\mathbf{x}) + \sum_{s \in \mathcal{S}} f_o(\mathbf{z}_s), \tag{EGSIP} \\ \text{s.t.} \quad & \forall \mathbf{y} \in \mathcal{Y}(\mathbf{x}) [\exists \mathbf{z} \in \mathcal{Z}_{epi}(\mathbf{x}, \mathbf{y}) : e_{epi} \leq 0] \end{aligned}$$

Generally, if the lower-level feasible set $\mathcal{Z}(\mathbf{x}, \mathbf{y})$ of the (RES_D) problem is defined by constraints of

the form $\mathbf{g}_z(\mathbf{x}, \mathbf{y}, \mathbf{z}) \leq \mathbf{0}$, a reformulation of the problem is required to ensure applicability of the ESIP algorithm (Djelassi, 2020). This reformulation moves the constraints $\mathbf{g}_z(\mathbf{x}, \mathbf{y}, \mathbf{z}) \leq \mathbf{0}$ into the objective function, which enables the medial level to identify \mathbf{y} that make the lower-level problem infeasible. However, in problem (EGSIP), the epigraph reformulation constraints $e_t(\mathbf{x}, \mathbf{y}, \mathbf{z}) - e_{epi} \leq 0 \ \forall t \in \mathcal{T}$ are always feasible if the bounds on e_{epi} are sufficiently large, which we can always guarantee by choosing the bounds appropriately. The guaranteed feasibility of the epigraph constraints allows us to omit the reformulation step for the epigraph reformulation constraints. Similarly, it is not necessary to move constraints of the form $\mathbf{g}_z(\mathbf{x}, \mathbf{z}) \leq \mathbf{0}$ into the objective function since \mathbf{y} cannot cause infeasibility of $\mathbf{g}_z(\mathbf{x}, \mathbf{z})$. Note that uncertainties typically occurring in energy system design problems are uncertain demand and uncertain generation by renewable energy sources, which enter the problem only in the energy balance, i.e., the objective function of the medial-level problem.

The next step is to form the ESIP relaxation. To this end, we first write problem (EGSIP) equivalently (Djelassi, 2020) as

$$\begin{aligned} \min_{\mathbf{x} \in \mathcal{X}, \mathbf{z}_s \in \mathcal{Z}_s(\mathbf{x}, \mathbf{y}_s)} \quad & f(\mathbf{x}) + \sum_{s \in \mathcal{S}} f_o(\mathbf{z}_s), \\ \text{s.t.} \quad & \forall \mathbf{y} \in \mathcal{Y}_{ref} [\exists \mathbf{z} \in \mathcal{Z}_{epi}(\mathbf{x}, \mathbf{y}) : e_{epi} \leq 0 \vee \mathbf{g}_y(\mathbf{x}, \mathbf{y}) > \mathbf{0}], \end{aligned}$$

where $\mathcal{Y}_{ref} = \{\mathbf{y} \in \mathbb{R}^{n_y} \mid \mathbf{h}_y(\mathbf{y}) = \mathbf{0}, \mathbf{g}_y(\mathbf{y}) \leq \mathbf{0}\}$ is the set of possible uncertainty realizations without the inequality constraints that depend on the upper-level variables \mathbf{x} , which instead have been moved into the logical constraint $e_{epi} \leq 0 \vee \mathbf{g}_y(\mathbf{x}, \mathbf{y}) > \mathbf{0}$. This logical constraint describes that either the medial-level problem is feasible and the energy supply gap is nonpositive or the medial-level problem is infeasible, i.e., the set of worst-case uncertainty realizations is empty. In either case, the upper-level problem is feasible. Furthermore, we assume here that the coupling equality constraints $\mathbf{h}_y(\mathbf{x}, \mathbf{y}) = \mathbf{0}$, if they were present, have been removed using the procedure described at the beginning of this Section.

To make the ESIP algorithms available in libDIPS (Zingler et al., 2023) applicable, the strictness of the inequality $-\mathbf{g}_y(\mathbf{x}, \mathbf{y}) < \mathbf{0}$ is relaxed, resulting in an ESIP problem:

$$\begin{aligned} \min_{\mathbf{x} \in \mathcal{X}, \mathbf{z}_s \in \mathcal{Z}_s(\mathbf{x}, \mathbf{y}_s)} \quad & f(\mathbf{x}) + \sum_{s \in \mathcal{S}} f_o(\mathbf{z}_s), \\ \text{s.t.} \quad & \forall \mathbf{y} \in \mathcal{Y}_{ref} [\exists \mathbf{z} \in \mathcal{Z}_{epi}(\mathbf{x}, \mathbf{y}) : e_{epi} \leq 0 \vee -\mathbf{g}_y(\mathbf{x}, \mathbf{y}) \leq \mathbf{0}], \end{aligned}$$

which can also be written as:

$$\begin{aligned} \min_{\mathbf{x} \in \mathcal{X}, \mathbf{z}_s \in \mathcal{Z}_s(\mathbf{x}, \mathbf{y}_s)} \quad & f(\mathbf{x}) + \sum_{s \in \mathcal{S}} f_o(\mathbf{z}_s), \\ \text{s.t.} \quad & \forall \mathbf{y} \in \mathcal{Y}_{ref} [\exists \mathbf{z} \in \mathcal{Z}_{epi}(\mathbf{x}, \mathbf{y}) : \min(e_{epi}, -g_{y,j}(\mathbf{x}, \mathbf{y}) \mid j \in \{1, \dots, n_{g_y}\}) \leq 0] \end{aligned} \quad (\text{ESIP REL})$$

Note that this relaxation is generally inexact. However, it is established in SIP literature that for all but degenerate cases, the relaxed problem should lead to the same objective value as the original problem [Mitsos and Tsoukalas \(2015\)](#).

For notational convenience, we define $g_e(\mathbf{x}, \mathbf{y}, \mathbf{z}) := \min(e_{epi}, -g_{y,j}(\mathbf{x}, \mathbf{y}) \mid j \in \{1, \dots, n_{g_y}\})$ and write [ESIP REL](#) as:

$$\begin{aligned} \min_{\mathbf{x} \in \mathcal{X}, \mathbf{z}_s \in \mathcal{Z}_s(\mathbf{x}, \mathbf{y}_s)} \quad & f(\mathbf{x}) + \sum_{s \in \mathcal{S}} f_o(\mathbf{z}_s), \\ \text{s.t.} \quad & \forall \mathbf{y} \in \mathcal{Y}_{ref} [\exists \mathbf{z} \in \mathcal{Z}_{epi}(\mathbf{x}, \mathbf{y}) : g_e(\mathbf{x}, \mathbf{y}, \mathbf{z}) \leq 0] \end{aligned} \quad (\text{ESIP})$$

The [\(ESIP\)](#) problem determines design decision variables \mathbf{x} and operational decision variables \mathbf{z}_s such that for all feasible uncertainty realizations \mathbf{y} in the set of possible uncertainty realizations \mathcal{Y}_{ref} there exist operational recourse actions \mathbf{z} so that the constraint $g_e(\mathbf{x}, \mathbf{y}, \mathbf{z}) \leq 0$ is satisfied, meaning that either $e_{epi} \leq 0$ is satisfied or one of the EGSIP constraints is violated, i.e., $-g_{y,j}(\mathbf{x}, \mathbf{y}) \leq 0$, and the set of uncertainty realizations of the EGSIP $\mathcal{Y}(\mathbf{x})$ is empty.

3 Limitations of the Feasibility Time-Step Heuristic

This section highlights how the feasibility time-step heuristic cannot rigorously provide robust designs for nonconvex problems. Specifically, we showcase in [Section 3.1](#) how the RESD approach can identify a robust design for a nonconvex problem while the feasibility time-step heuristic ([Bahl et al., 2016](#); [Teichgraeber et al., 2020](#)) fails. [Section 3.2](#) shows the cases for which the feasibility time-step heuristic yields robust designs. Finally, in [Section 3.3](#), we present an extension to the RESD approach that improves performance for problems with convex lower-level problem.

3.1 MILP Example

Ensuring operability for all historical data may not be enough to obtain a robust design if the operational problem is nonconvex. SIPs with nonconvex lower-level problems are challenging to solve and cannot, in

general, be reformulated as finite optimization problems (Djelassi et al., 2021). The reformulation into a tractable finite optimization problem requires the equations and uncertainty set to fulfill special criteria (Bertsimas et al., 2011). MILPs are nonconvex problems and are extensively used in energy system design (Pfenninger et al., 2014). Therefore, we use a small MILP example that mimics an energy system to demonstrate the shortcomings of the feasibility time-step heuristic and solve it using the RESD approach.

The MILP problem reads

$$\begin{aligned} \min_{(x_1, x_2) \in [0, 100]^2} \quad & 2x_1 + x_2, \\ \text{s.t.} \quad & \forall y_1 \in [0, 100] [\exists (z_1, z_2, b) \in \mathcal{Z}(x_1, x_2, y_1) : y_1 - z_1 - z_2 \leq 0], \end{aligned} \quad (\text{MILP RESD})$$

with the feasible set

$$\begin{aligned} \mathcal{Z}(x_1, x_2, y_1) = \{ (z_1, z_2) \in [0, 100]^2, b \in \{0, 1\} \mid & z_1 - x_1 \leq 0 \wedge z_2 - bx_2 \leq 0 \wedge \\ & 0.2bx_2 - z_2 \leq 0 \wedge y_1 - z_1 - z_2 = 0 \}. \end{aligned}$$

In (MILP RESD), x_1 and x_2 represent abstract component capacities, y_1 an uncertain demand, and z_1 and z_2 component outputs, while b models on/off decisions for component 2 to account for the minimal part load restriction of that component. Compared with Component 1, Component 2 is half as expensive to install but has a minimum part load, below which the component has to be shut off.

For simplicity, we assume cost and demand data without reference to real-world data. Specifically, Component 1 is assumed to cost 2 units, and Component 2 is assumed to cost 1 unit. Demand is assumed to be in the range between 0 and 100 units and has to be met exactly without curtailment of excess power.

Note that the coupling equality constraint $y_1 - z_1 - z_2 = 0$, which represents the no-curtailment constraint, can be handled by applying the approach described in Section 2.2, i.e., we solve the equality constraint explicitly for z_2 and substitute $z_2 = y_1 - z_1$ to obtain the following problem:

$$\begin{aligned} \min_{(x_1, x_2) \in [0, 100]^2} \quad & 2x_1 + x_2, \\ \text{s.t.} \quad & \forall y_1 \in [0, 100] [\exists (z_1, b) \in \mathcal{Z}_{feas}(x_1, x_2, y_1) : 0 \leq 0], \end{aligned} \quad (\text{MILP FEAS})$$

with the feasible set

$$\mathcal{Z}_{feas}(x_1, x_2, y_1) = \{ z_1 \in [0, 100], b \in \{0, 1\} \mid z_1 - x_1 \leq 0 \wedge y_1 - z_1 - bx_2 \leq 0 \wedge 0.2bx_2 - y_1 + z_1 \leq 0 \}.$$

When substituting $z_2 = y_1 - z_1$ into the SIP constraint, we obtain the trivial constraint $0 \leq 0$, which is always satisfied if the feasible set $\mathcal{Z}_{feas}(x_1, x_2, y_1)$ is not empty. Hence, (MILP FEAS) ensures that the lower-level feasible set is not empty.

The lower-level feasible set $\mathcal{Z}_{feas}(x_1, x_2, y_1)$ depends on the uncertain variable y_1 . As described in Section 2.2, we remove this dependency by moving the constraints into the objective function of the medial- and lower-level problem, i.e.,

$$\begin{aligned} \min_{(x_1, x_2) \in [0, 100]^2} \quad & 2x_1 + x_2, & (\text{MILP ESIP REF}) \\ \text{s.t.} \quad & \forall y_1 \in [0, 100] [\exists (z_1, b) \in \mathcal{Z}_{ref}(x_1, x_2) : \max\{y_1 - z_1 - bx_2, 0.2bx_2 - y_1 + z_1\} \leq 0], \end{aligned}$$

with the feasible set

$$\mathcal{Z}_{ref}(x_1) = \{z_1 \in [0, 100], b \in \{0, 1\} \mid z_1 - x_1 \leq 0\}.$$

and solve it using the ESIP algorithm implemented in libDIPS (Zingler et al., 2023). The involved sub-problems and the solver settings can be found in Section 1 and Table 2 of the supplementary material, respectively.

We obtain an optimal system design with $x_1 = 16.60$ and $x_2 = 83.40$, i.e., the capacity of the more expensive Component 1 is roughly 20 % of the capacity of Component 2. The fact that the more expensive Component 1 is built allows the system to satisfy the demand below the minimal part load of Component 2.

If only the vertices of the uncertain demand set $\{0, 100\}$ had been considered, the optimal solution would have been $x_1 = 0$ and $x_2 = 100$. However, this solution is not robust to certain possible intermediate demands. For example, the demand $y_1 = 15$ lies below the minimal part load of Component 2, i.e., $0.2 \cdot 100 = 20$. Since Component 1 would have been installed, this demand could not be satisfied.

Note that the nonconvexity introduced by the minimal part load of Component 2 would not lead to infeasibility without the no-curtailment assumption. If curtailment were allowed, Component 2 could be operated at minimal part load for demands smaller than its minimal part load. Consequently, the minimal part load could be neglected in the medial-level problem, effectively removing the nonconvexity. Thus, nonconvexities do not necessarily lead to worst-case scenarios that lie in-between historical scenarios. However, the example highlights that care must be taken when applying the feasibility time-step heuristic (Bahl et al., 2016; Teichgraber et al., 2020) to nonconvex problems.

3.2 When Considering Historical Data is Sufficient

In the previous section, we highlighted how the feasibility time-step heuristic (Bahl et al., 2016; Teichgraber et al., 2020) may fail for nonconvex problems. However, there are special cases for which the heuristic yields designs that are identical to the ones found by the RESD approach using the convex hull bounding the full dimensional uncertainty space. In these special cases, the objective function $g_e(\mathbf{x}, \mathbf{y}, \mathbf{z})$ and the constraints of the lower-level problem need to be such that worst-case scenarios lie at an extreme point of \mathcal{Y}_{ref} . An analogy to this is that the maximum of a convex function lies at an extreme point of its domain. The identified designs are then robust to all uncertainty realizations in the convex hull of the considered historical data.

Worst-case scenarios can then be identified by solving the embedded (MAXMIN) problem, i.e.,

$$\max_{\mathbf{y} \in \mathcal{Y}_{ref}} \min_{\mathbf{z} \in \mathcal{Z}_{epi}(\mathbf{x}, \mathbf{y})} g_e(\mathbf{x}, \mathbf{y}, \mathbf{z}), \quad (\text{MAXMIN})$$

using vertex enumeration (Halemane and Grossmann, 1983), i.e., the vertices of the feasible set of uncertainty realizations \mathcal{Y}_{ref} are enumerated, and the operational problem is solved for each vertex. It is thus sufficient to examine the historical data that constitute the vertices of the convex hull and unnecessary to consider the entire historical data set, as it is done in the feasibility time-step heuristic.

There are two special cases for which Halemane and Grossmann (1983) and Bialas and Karwan (1982) have proven that the worst-case scenarios lie on the vertices of the feasible set and for which the feasibility time-step heuristic thus leads to robust designs: (i) if the semi-infinite constraint $g_e(\mathbf{x}, \mathbf{y}, \mathbf{z})$ is jointly convex in \mathbf{y} and \mathbf{z} and all other lower-level constraints are convex in \mathbf{z} (Halemane and Grossmann, 1983), and (ii) if both the medial-level and the lower-level problem of the (RESD) problem are linear, i.e., the objectives and constraints are linear and consequently the embedded MAXMIN problem is a bilevel linear program (BLLP) (Bialas and Karwan, 1982).

3.3 Lifting Approach for Convex Lower-Level Problems

Finally, we introduce a lifting approach to improve the computational performance of the RESD approach that is applicable if the lower-level problem is convex, i.e., the operational problem is convex. The motivation for this reformulation is that solving (ESIP) using the ESIP algorithm proposed by Djelassi and Mitsos (2021), which is based on the Blankenship and Falk (1976) algorithm, proved to be computationally slow in our preliminary investigations. Specifically, we found that the majority of the CPU time to solve the ESIP was spent on the solution of the embedded optimization problem (MAXMIN), which

is equivalent to the semi-infinite existence constraint of (ESIP), i.e., $\forall \mathbf{y} \in \mathcal{Y}_{ref} [\exists \mathbf{z} \in \mathcal{Z}_{epi}(\mathbf{x}, \mathbf{y}) : g_e(\mathbf{x}, \mathbf{y}, \mathbf{z}) \leq 0]$.

The lifting approach described in Diehl et al. (2013) allows us to reformulate (MAXMIN) as a single-level nonlinear program (NLP). To this end, we first reformulate (MAXMIN) as a SIP by writing its epigraph reformulation with the auxiliary variable ϕ (Stein, 2003):

$$\begin{aligned} & \max_{\mathbf{y} \in \mathcal{Y}_{ref}, \phi} \phi, \\ \text{s.t.} \quad & \phi - g_e(\mathbf{x}, \mathbf{y}, \mathbf{z}) \leq 0 \quad \forall \mathbf{z} \in \mathcal{Z}_{epi}(\mathbf{x}, \mathbf{y}) \end{aligned} \tag{ES}$$

We then employ the lifting method (Diehl et al., 2013) to reformulate (ES) into the NLP

$$\begin{aligned} & \max_{\mathbf{y} \in \mathcal{Y}_{ref}, \mathbf{z} \in \mathcal{Z}_{epi}(\mathbf{x}, \mathbf{y}), \phi, \boldsymbol{\lambda}, \boldsymbol{\mu}} \phi, \\ \text{s.t.} \quad & \phi - \mathcal{L}(\mathbf{x}, \mathbf{y}, \mathbf{z}, \boldsymbol{\lambda}, \boldsymbol{\mu}) = 0, \\ & \nabla_{\mathbf{z}} \phi - \nabla_{\mathbf{z}} \mathcal{L}(\mathbf{x}, \mathbf{y}, \mathbf{z}, \boldsymbol{\lambda}, \boldsymbol{\mu}) = \mathbf{0}, \\ & \boldsymbol{\mu} \geq \mathbf{0}, \\ & \boldsymbol{\mu}^\top \mathbf{g}_z(\mathbf{x}, \mathbf{y}, \mathbf{z}) = 0, \end{aligned}$$

with Lagrange multipliers $\boldsymbol{\lambda}$ and $\boldsymbol{\mu}$ and

$$\mathcal{L}(\mathbf{x}, \mathbf{y}, \mathbf{z}, \boldsymbol{\lambda}, \boldsymbol{\mu}) = g_e(\mathbf{x}, \mathbf{y}, \mathbf{z}) + \boldsymbol{\lambda}^\top \mathbf{h}_z(\mathbf{z}) + \boldsymbol{\mu}^\top \mathbf{g}_z(\mathbf{x}, \mathbf{y}, \mathbf{z}).$$

Note that $\nabla_{\mathbf{z}} \phi = 0$ and by substituting ϕ in the objective function using $\phi = \mathcal{L}(\mathbf{x}, \mathbf{y}, \mathbf{z}, \boldsymbol{\lambda}, \boldsymbol{\mu})$ we end up with the single-level problem:

$$\begin{aligned} & \max_{\mathbf{y} \in \mathcal{Y}_{ref}, \mathbf{z} \in \mathcal{Z}_{epi}(\mathbf{x}, \mathbf{y}), \boldsymbol{\lambda}, \boldsymbol{\mu}} \mathcal{L}(\mathbf{x}, \mathbf{y}, \mathbf{z}, \boldsymbol{\lambda}, \boldsymbol{\mu}), \\ \text{s.t.} \quad & \nabla_{\mathbf{z}} \mathcal{L}(\mathbf{x}, \mathbf{y}, \mathbf{z}, \boldsymbol{\lambda}, \boldsymbol{\mu}) = \mathbf{0}, \\ & \boldsymbol{\mu} \geq \mathbf{0}, \\ & \boldsymbol{\mu}^\top \mathbf{g}_z(\mathbf{x}, \mathbf{y}, \mathbf{z}) = \mathbf{0} \end{aligned} \tag{NLP}$$

The objective is nonlinear because of the multiplication of the Lagrange multipliers $\boldsymbol{\mu}$ and $\boldsymbol{\lambda}$ with the constraints $\mathbf{g}_z(\mathbf{x}, \mathbf{y}, \mathbf{z})$ and $\mathbf{h}_z(\mathbf{z})$. Note that, contrary to Diehl et al. (2013), we added the nonlinear complementarity constraints $\boldsymbol{\mu}^\top \mathbf{g}_z(\mathbf{x}, \mathbf{y}, \mathbf{z}) = \mathbf{0}$ since we found this to help convergence in our case study

(cf. Section 4). This is an unexpected result since a major motivation of the lifting approach is to avoid the complementarity constraints, which are numerically poorly behaved (Scheel and Scholtes, 2000).

Finally, by replacing (MAXMIN) with its single-level reformulation (NLP), we obtain the SIP reformulation of the (RESL), i.e.,

$$\begin{aligned} \min_{\mathbf{x} \in \mathcal{X}, \mathbf{z}_s \in \mathcal{Z}_s(\mathbf{x})} \quad & f(\mathbf{x}) + \sum_{s \in \mathcal{S}} f_o(\mathbf{z}_s), \\ \text{s.t.} \quad & \mathcal{L}(\mathbf{x}, \mathbf{w}) \leq 0 \quad \forall \mathbf{w} \in \mathcal{W}(\mathbf{x}), \end{aligned} \tag{RESL SIP}$$

with

$$\begin{aligned} \mathcal{W}(\mathbf{x}) = \{ & \mathbf{y} \in \mathcal{Y}_{ref}, \mathbf{z} \in \mathcal{Z}_{ept}(\mathbf{x}, \mathbf{y}), \boldsymbol{\lambda}, \boldsymbol{\mu} \mid \\ & \nabla_{\mathbf{z}} \mathcal{L}(\mathbf{x}, \mathbf{y}, \mathbf{z}, \boldsymbol{\lambda}, \boldsymbol{\mu}) = \mathbf{0}, \boldsymbol{\mu} \geq \mathbf{0}, \\ & \boldsymbol{\mu}^\top \mathbf{g}_l(\mathbf{x}, \mathbf{y}, \mathbf{z}) = \mathbf{0} \}. \end{aligned}$$

(RESL SIP) can be solved using the implementation of the Blankenship & Falk algorithm (Blankenship and Falk, 1976) available in libDIPS (Zingler et al., 2023).

4 La Palma Energy System

We now analyze how close the lower-dimensional RESL problem approximates the costs of the full-dimensional problem as well as the performance of the RESL approach using the example of determining a robust energy system design for the island of La Palma in the Canary Islands. La Palma is an example of an isolated energy system with significant decarbonization potential. Isolated energy systems are defined by a lack of connection to a superordinate energy grid and, consequently, a necessity for self-sufficiency in electricity production. Due to their maturity and reliability, diesel engines have been the electricity generators of choice for many isolated systems (Kennedy et al., 2017). As of 2021, only 20 % of gross electricity production in the whole Canary Islands was supplied by renewable sources, highlighting the presently strong reliance on fossil fuels (Gobierno de Canarias, 2023a). Furthermore, the Canary Islands have a high availability of renewable energy resources, especially solar (Meschede et al., 2016), and plans to decarbonize their economy and achieve carbon neutrality by 2040 (Gobierno de Canarias, 2023b) have been announced.

We consider the following system components: PV units, wind turbines, diesel generators, and battery systems. We neglect to model the electricity distribution system and the related transmission losses to

keep the computational complexity manageable; thus, all system components are directly connected to a single node to supply the island’s energy demand.

We use data for wind speed and global irradiance obtained from the Photovoltaic Geographical Information System (PVGIS) by the European Union ([European Commission, 2022](#); [Huld et al., 2012](#)). Furthermore, electricity demand data was aggregated from the Spanish electricity system operator [Red Eléctrica de España \(2024\)](#). The data covers the timespan from 2013 to 2019 and is separated into single-day periods with an hourly resolution. We use 15 representative scenarios in the approximation of the operational costs, as this number leads to a decent approximation of the load curve (see supplementary materials, Figure 2). Detailed information about the case study, such as the modeling of the individual components, determination of cost parameters, and the overall problem formulation, is provided in Section 2 of the supplementary materials.

The resulting RESD problem has linear medial- and lower-level problems. Hence, the lifting approach (cf. Section 3.3), the vertex enumeration (cf. Section 3.2), and thus also the feasibility time-step heuristic ([Bahl et al., 2016](#); [Teichgraeber et al., 2020](#)) are applicable. We utilize the latter as a reference to solve the full-dimensional problem and compare the solution to those of the RESD approach with different degrees of dimensionality reduction. We do not compare the computational performance of the feasibility time-step heuristic with that of the RESD approach, as the RESD approach is generally applicable, i.e., for nonconvex problems, whereas the feasibility time-step heuristic yields guaranteed robust designs only in the special cases described in Section 3.2.

The full problem formulation and the application of the reformulation steps described in Section 2 to transform the embedded optimization problem into a single-level NLP are provided in the supplementary materials in Sections 2.2 & 2.4. The resulting (ESIP) and (RESIP) are solved with the Blankenship & Falk-based ESIP algorithm and the Blankenship & Falk algorithm, respectively, using the implementation in libDIPS ([Zingler et al., 2023](#)) and the Gurobi solver version 11.0 ([Gurobi Optimization, LLC, 2024](#)). We use a desktop computer with a 4-core/4-thread Intel i5-4570 CPU with 3.2 GHz/3.6 GHz base/turbo frequency and 16 GB of RAM running Microsoft Windows 10 Enterprise version 10.0.17763. Optimization settings for libDIPS and Gurobi deviating from the default values are given in Section 3 of the supplementary materials; all 4 cores were allocated to the numerical experiments.

4.1 Optimal Robust Design

First, we briefly analyze the robust design resulting from the RESD approach and compare it to La Palma’s current energy system. Figure 2 shows the mean and the standard deviation of the daily electricity

demand. Additionally, the 15 representative scenarios used to approximate the operational costs are shown. The demand varies significantly over the course of a day, with a multiple-hour-long peak in the middle of the day between 08:00 and 12:00 and a sharp peak in the evening around 20:00. The demand data varies between 0.2 MW and 44.8 MW, with the low value of 0.2 MW being associated with a power outage that occurred on December 11th, 2013.

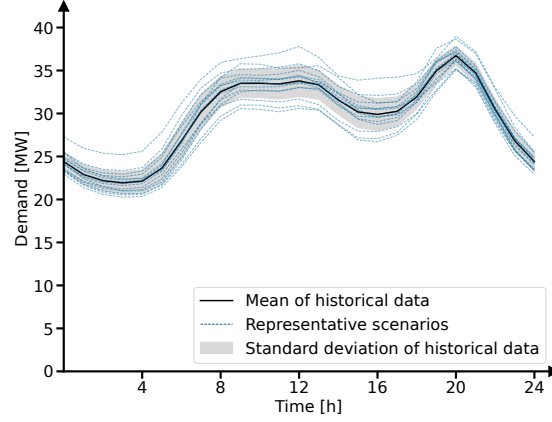


Fig. 2. Mean and standard deviation of the daily historical electricity demand on the island of La Palma in 2013-2019. Demand data were obtained from the Spanish electricity distribution system operator [Red Eléctrica de España \(2024\)](#). Furthermore, the 15 representative scenarios used to compute the operational costs are depicted as dashed lines. There is significant variation in demand over the course of a day, with a wide peak during the morning and a sharp peak in the evening.

Figure 3 shows the currently installed capacities as well as the capacities of the robust design obtained by the RESD approach using 16 time steps and 9 principal components.

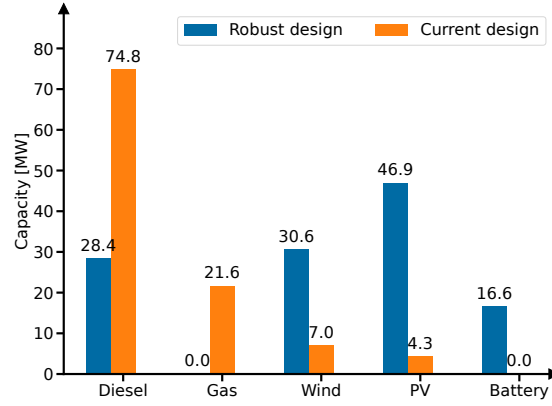


Fig. 3. Installed component capacities for the robust design (blue) identified by the RESD approach using 16 time steps and 9 principal components. For comparison, the currently installed capacities (orange) (Gobierno de Canarias, 2023a) are shown. The current design has much higher conventional generation capacity. However, plans to switch to higher renewable electricity generation have already been announced (Gobierno de Canarias, 2023b). Note that we did not consider possible component failures in the RESD approach, and hence do not have backup capacities, which are considered in the current design.

The total annualized costs (TAC) of the RESD design amount to 28.0 M€/yr and are comprised of 19.2 M€/yr of capital expenses and 8.8 M€/yr of operational expenses. The average cost of electricity generation is 105.6 €/MWh, compared to the actual average cost of electricity generation in the entire Canary Islands of 161.5 €/MWh in 2021 (Gobierno de Canarias, 2023a). Note that the current energy system has an overcapacity of conventional diesel generators due to some of the generation capacity being held back as a backup. In the RESD approach, we do not take into account possible component failures.

In the robust design, the majority of electricity is produced by wind turbines with 50.8%, followed by solar with 41.2%, and diesel with 8.0%. Renewable resources are preferred over diesel since they have lower variable operational costs. The high variable operational costs of diesel engines are primarily driven by the price of fuel and the costs of dispatch emission rights, which are described in Section 2.3 of the supplementary material. Compared to the current design, the RESD design exhibits a much higher share of renewable generation, with the renewable energy penetration reaching 92.0%. In comparison, only 10.3% of gross electricity production in La Palma was supplied by renewable sources in 2021 (Gobierno de Canarias, 2023a).

4.2 Performance and Accuracy

We run the La Palma case study for different numbers of time steps and principal components (PCs). Varying the latter parameter allows us to determine how the dimensionality reduction influences the

computational performance and the accuracy of the obtained results. We always use five random seeds for the Gurobi optimizer (Gurobi Optimization, LLC, 2024) and average the obtained solution times since solution times can vary strongly with random seeds depending on the nodes explored by the branch and bound algorithm. We measure the solution time by taking the ‘CPU time’ reported by libDIPS (Zingler et al., 2023), which is the sum of the wall-clock times reported by Gurobi (Gurobi Optimization, LLC, 2024) for all sub-problems. Note that we did not account for the time it takes to calculate the convex hull in the performance evaluations. As mentioned in Section 2.1, with larger latent space dimensionality, the time to compute the convex hull can become significant compared to the solution time. Hence, we limited the maximum number of principal components in our numerical experiments to 9.

Figure 4 shows the average solution time for the ESIP and the lifting approach for different numbers of PCs and time steps.

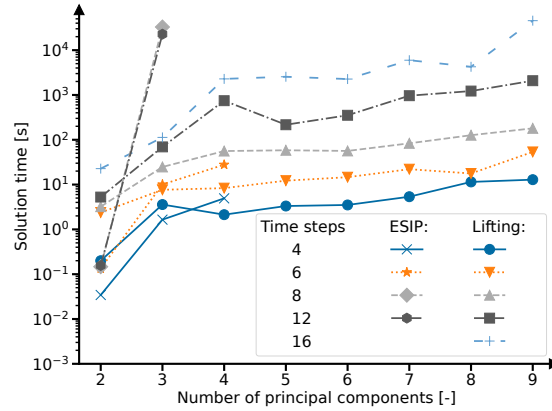


Fig. 4. Average solution times in logarithmic scale for the ESIP and the lifting approach. The average solution time in seconds is plotted against the number of principal components (PCs) for varying numbers of time steps. The solution time increases both with an increasing number of PCs and time steps. The lifting approach scales better with an increasing number of PCs than the ESIP approach.

As expected, the solution time increases with an increasing number of time steps and PCs. The ESIP approach shows a very strong increase in the solution time with an increasing number of PCs. In fact, we could not obtain results for four or more components with the ESIP approach since the run times became too long. The lifting approach outperforms the ESIP approach if more than two PCs are used. There is a significant increase in solution time between two and three components. Afterward, solution time increases more slowly with an increasing number of components. Furthermore, higher temporal resolutions strongly increase solution times.

The top of Figure 5 shows the optimal TACs of the energy system designs obtained using the lifting approach plotted against the number of PCs for a varying number of time steps. As a reference, the

results obtained using the feasibility time-step heuristic (Bahl et al., 2016; Teichgraeber et al., 2020) described in Section 3.2 are shown. The bottom shows the explained variance ratio.

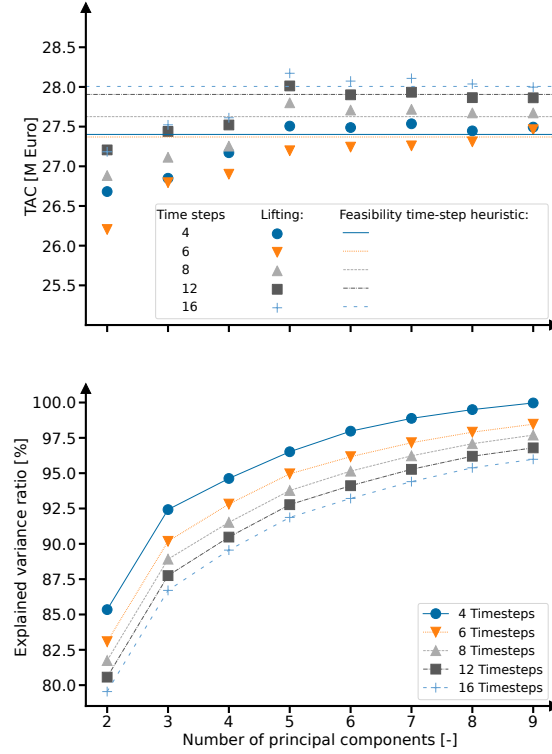


Fig. 5. Optimal total annualized cost (TAC) of energy system designs obtained using the lifting approach against the number of principal components (PCs) for varying number of time steps (top). Dashed lines show results obtained with the feasibility time-step heuristic (Bahl et al., 2016; Teichgraeber et al., 2020) discussed in Section 3.2. For a low number of PCs, a significant approximation error can be seen. If the number of PCs is chosen sufficiently large, i.e., greater than or equal to 5, the TAC of full-dimensional problems is approximated closely by the RESD approach. Explained variance ratio plotted against the number of PCs for a varying number of time steps (bottom). A small number of PCs can explain a majority of the variance in the historical data.

If the number of PCs is small, the RESD designs have lower TACs than the designs resulting from the heuristic. This indicates that, for a small number of PCs, the truncation error from the dimensionality reduction leads to designs that are not robust. With an increasing number of PCs, the TAC of the RESD designs quickly approach those of the designs resulting from the heuristic. In some cases, the TACs of the RESD designs exceed those of the designs obtained by the heuristic, indicating that the truncation error can also lead to overly robust designs. Note that relatively few PCs are needed to account for a majority of the variance in the historical data. With 5 PCs, more than 90 % of the variance are explained for all time resolutions. We observe that the TAC of the full-dimensional problem are approximated closely for all time resolutions if the number of PCs is chosen such that the explained variance is above 95 %.

Figure 6 shows the energy supply gap over the number of PCs for different time resolutions. The energy supply gap is calculated by solving the operational problem for each historical data point and selecting the maximum constraint violation.

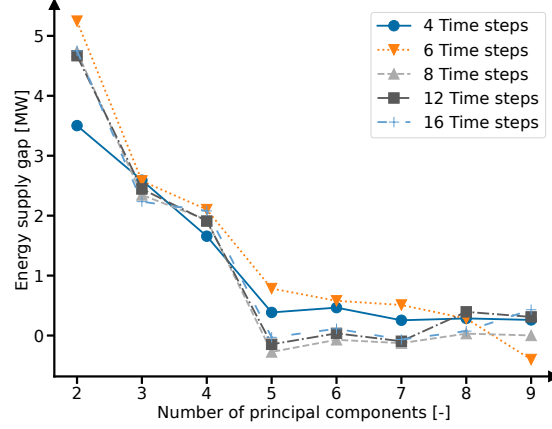


Fig. 6. The maximum energy supply gap for RESD designs with different time resolutions obtained using the lifting approach, calculated by solving the operational problem for all historical data points, is plotted against the number of principal components (PCs). The supply gap is large for a small number of PCs, showing that these designs are not robust. The energy supply gap decreases quickly with an increase in the number of PCs and levels off close to 0 MW at 5 PCs, indicating robust designs.

For a small number of PCs, the energy supply gap is large, i.e., in the order of multiple megawatts, showing that these designs are not robust. This finding highlights the tradeoff between a sufficiently accurate approximation of the time-series data and the computational performance. Importantly, the energy supply gap decreases quickly with an increase in the number of PCs and levels off around 5 PCs. In fact, for 48 dimensional data, i.e., 16 time steps and 3 quantities (solar, wind, demand), 6 PCs are sufficient to achieve an appropriate approximation of the full-dimensional problem and hence a robust design. In some cases, the energy supply gap even becomes negative, indicating an overly robust design. This is in accordance with the observation that the TACs for these numbers of PCs are higher than the respective TACs for the designs obtained by the heuristic.

Choosing the right dimensionality of the latent space is difficult in the case of a nonconvex problem. However, we note that the energy supply gap approaches zero for designs that were obtained with a latent space dimensionality that covers more than 95 % of the variance in the historical data. Hence, the explained variance ratio may be used as an indicator to decide on an appropriate dimensionality of the latent space.

5 Conclusion

Uncertainties introduced by VRES should be incorporated into the design of energy systems. Previously *a priori* heuristics, e.g., statistical selection of extreme periods (Domínguez-Muñoz et al., 2011), or optimization-based heuristics, e.g., the feasibility time-step heuristic (Bahl et al., 2016; Teichgraeber et al., 2020), have been proposed. However, *a priori* methods cannot identify extreme periods specific to the energy system because they are agnostic to its design. Moreover, optimization-based heuristics may fail if the design problem exhibits a nonconvex operational problem, e.g., a MILP resulting from the need to model minimal part loads.

We present the robust energy system design (RESD) approach, a rigorous but computationally intense approach to identify extreme scenarios during the design optimization. Specifically, we introduce a semi-infinite existence constraint to the energy system design problem to ensure robustness with respect to uncertainties, resulting in a tri-level optimization problem.

Our RESD approach for the identification of worst-case scenarios during optimization can be seen as a generalization of the finite optimization problem corresponding to the feasibility time-step heuristic (Bahl et al., 2016; Teichgraeber et al., 2020), which determines the constraint violation for all historical scenarios and iteratively adds scenarios with infeasible time steps as extreme scenarios. However, as we have discussed, it is only sufficient to check operability with the historical data, or more specifically, all the scenarios that define the boundary of the convex hull of the historical data, in the case of linear medial- and lower-level problems or jointly convex medial- and lower-level problems. The computational performance of the iterative feasibility time-step heuristic could potentially be improved by using a preprocessing step to identify and discard some or all data points in the interior. In contrast, our RESD approach is dedicated to the more general nonconvex case. The MILP example in Section 3.1 demonstrates how components with minimal part load in combination with a no-curtailment constraint can lead to worst-case scenarios that lie between historical data and not on the vertices of the uncertainty set. Future work should examine to which extent the worst-case scenarios for realistic multi-energy systems, which allow for some curtailment and/or contain storage components, also do not lie on the vertices of the uncertainty set.

Different uncertainty-bounding methods can be used in the RESD approach. In the present contribution, we consider the convex hull of the historical data as the possible uncertainty set, taking advantage of the fact that the describing equations are linear. Still, the computational effort for solving the RESD problem increases quickly with an increasing number of time steps.

Computational tractability can be improved by leveraging dimensionality reduction techniques such

as principal component analysis (PCA). While we observe that robust designs can be obtained even in the presence of rather aggressive dimensionality reduction, the use of PCA inherently introduces an approximation error that can lead to overly or underly robust designs. A suitable dimensionality of the latent space must be found empirically, and in the nonconvex case, a rigorous criterion for validating the robustness of an obtained design is missing. However, the explained variance ratio can be used as an indicator in guiding the selection of an appropriate latent space dimensionality. Specifically, we found designs obtained with a latent space dimensionality covering more than 95 % of the variance of the historical data to yield TACs that are close to the TAC of the full-dimensional design.

Although the lifting approach can improve performance if the considered design problem has an embedded convex operational problem, the applicability of the RESD approach is currently limited to small problems due to the involved computational intensity. Furthermore, we found that including the complementarity constraints improves the performance of the lifting approach. This is an unexpected result, and it should be investigated if this holds generally. Wider applicability of our approach could be enabled by faster methods for solving hierarchical programs. For example, the approach by [Seidel and Küfer \(2022\)](#) that improves the rate of convergence of the adaptive discretization approach could reduce the long solution times of the embedded MaxMin problem. Furthermore, the integration of bounding approaches that can handle nonconvexities in the historical data, e.g., holes, as well as the use of nonlinear dimensionality reduction techniques, e.g., autoencoders ([Kramer, 1991](#)), should be investigated.

Declarations

Ethics Approval and Consent to Participate

Not applicable.

Consent for Publication

Not applicable.

Funding

This work was performed as part of the Helmholtz School for Data Science in Life, Earth and Energy (HDS-LEE) and received funding from the Helmholtz Association of German Research Centers.

The authors gratefully acknowledge the financial support of the Kopernikus project SynErgie by the German Federal Ministry of Education and Research (BMBF) and the project supervision by the project

management organization Projektträger Jülich (PtJ).

Availability of Data and Materials

The cost parameters for the La Palma case study are collected in Table 1 in the supplementary material, and a detailed description of how they were obtained can be found in Section 2.3 of the supplementary material. The solar irradiance and wind speed data used in the La Palma case study are available at https://re.jrc.ec.europa.eu/pvg_tools/en/. The demand data for La Palma island is available at https://demanda.ree.es/visiona/canarias/la_palma5m/tablas. The wind turbine power curve data for an Enercon E-82 E2 turbine was used. While the data is no longer available on the official manufacturer site, a copy of the data sheet is accessible at https://catalystresearch.wordpress.com/wp-content/uploads/2013/11/enercon_pu_en.pdf.

Competing Interests

The authors have no relevant financial or non-financial interests to disclose.

Authors' Contributions

Conceptualization: M.W., E.C., A.M., M.D.; Methodology: M.W.; Software: M.W.; Formal analysis and investigation: M.W.; Visualization: M.W.; Writing - original draft preparation: M.W.; Writing - review and editing: E.C., A.M., M.D.; Funding acquisition: A.M., M.D.; Supervision: A.M., M.D.

Acknowledgements

During the preparation of this work, M.W. used Grammarly to correct grammar and spelling and improve the writing style. After using this tool, all authors reviewed and edited the content as needed and take full responsibility for the content of the publication.

Nomenclature

Throughout the manuscript, scalar-valued quantities are denoted in regular font, e.g., x , vector-valued quantities are denoted in bold font, e.g., \mathbf{x} , and set-valued quantities are denoted in calligraphic font, e.g., \mathcal{X} .

Abbreviations

BLLP	bi-level linear program
ESIP	existence-constrained semi-infinite program
EGSIP	existence-constrained generalized semi-infinite program
GSIP	generalized semi-infinite program
MILP	mixed-integer linear program
MW	megawatt
NLP	nonlinear program
RES	robust energy system design
PC	principal component
PCA	principal component analysis
PV	photo voltaic
SIP	semi-infinite program
TAC	total annualized cost
VRES	variable renewable energy sources

Greek Symbols

λ	Lagrange multiplier for equality constraints
μ	Lagrange multiplier for inequality constraints
ϕ	auxiliary variable

Latin Symbols

b	binary variable for on/off decision
e	energy supply gap
e_{epi}	auxiliary variable for energy supply gap
g	inequality constraint
\mathbf{g}	vector of inequality constraints
h	equality constraint
\mathbf{h}	vector of equality constraints
\mathcal{L}	Lagrangian function
n	number
\mathcal{S}	set of representative scenarios
\mathcal{T}	set of time steps
\mathbf{w}	vector of variables for single-level NLP
\mathcal{W}	feasible set of variables for single-level NLP
x	design variable
\mathbf{x}	vector of design variables
\mathcal{X}	feasible set of design variables
y	uncertain variable
\mathbf{y}	vector of uncertain variables
$\tilde{\mathbf{y}}$	vector of dependent uncertain variables
$\bar{\mathbf{y}}$	vector of independent uncertain variables
\mathcal{Y}	feasible set of uncertain variables
z	operational variable
\mathbf{z}	vector of operational variables
\mathcal{Z}	feasible set of operational variables

Subscripts

d	data points
e	energy supply gap
en	energy system
eq	equations
i	index
j	index
epi	epigraph reformulation
o	operational costs
p	principal components
ref	reformulation
s	representative scenarios
t	time step
x	design variables
y	uncertain variables
z	operational variables

References

- Avis, D., Bremner, D., and Seidel, R. (1997). How good are convex hull algorithms? *Computational Geometry*, 7(5):265–301.
- Bahl, B., Kümpel, A., Lampe, M., and Bardow, A. (2016). Time-series aggregation for synthesis of distributed energy supply systems by bounding error in operational expenditure. In Kravanja, Z. and Bogataj, M., editors, *Computer Aided Chemical Engineering*, volume 38 of *26 European Symposium on Computer Aided Process Engineering*, pages 793–798. Elsevier.
- Bahl, B., Lützow, J., Shu, D., Hollermann, D. E., Lampe, M., Hennen, M., and Bardow, A. (2018). Rigorous synthesis of energy systems by decomposition via time-series aggregation. *Computers & Chemical Engineering*, 112:70–81.
- Barone, G., Buonomano, A., Forzano, C., Giuzio, G. F., and Palombo, A. (2021). Supporting the Sustainable Energy Transition in the Canary Islands: Simulation and Optimization of Multiple Energy System Layouts and Economic Scenarios. *Frontiers in Sustainable Cities*, 3:685525.

- Baumgärtner, N. J., Temme, F., Bahl, B., Hennen, M. R., Hollermann, D. E., and Bardow, A. (2019). RiSES4 : Rigorous Synthesis of Energy Supply Systems with Seasonal Storage by relaxation and time-series aggregation to typical periods. In *Proceedings of the International Conference on Efficiency, Cost, Optimization, Simulation and Environmental Impact of Energy Systems (ECOS 2019)*, pages 263–274, Gliwice. Institute of Thermal Technology.
- Ben-Tal, A., El Ghaoui, L., and Nemirovski, A. S. (2009). *Robust Optimization*. Princeton Series in Applied Mathematics. Princeton University Press, Princeton.
- Ben-Tal, A. and Nemirovski, A. (2002). Robust optimization – methodology and applications. *Mathematical Programming*, 92(3):453–480.
- Bertsimas, D., Brown, D. B., and Caramanis, C. (2011). Theory and Applications of Robust Optimization. *SIAM Review*, 53(3):464–501.
- Bialas, W. and Karwan, M. (1982). On two-level optimization. *IEEE Transactions on Automatic Control*, 27(1):211–214.
- Biegler, L. and Grossmann, I. (2004). Retrospective on optimization. *Computers and Chemical Engineering*, 28(8):1169–1192.
- Birge, J. R. and Louveaux, F. (2011). *Introduction to Stochastic Programming*. SpringerLink Bücher. Springer New York, New York, NY.
- Blankenship, J. W. and Falk, J. E. (1976). Infinitely constrained optimization problems. *Journal of Optimization Theory and Applications*, 19(2):261–281.
- Bünning, F., Wetter, M., Fuchs, M., and Müller, D. (2018). Bidirectional low temperature district energy systems with agent-based control: Performance comparison and operation optimization. *Applied Energy*, 209:502–515.
- Campo, P. J. and Morari, M. (1987). Robust Model Predictive Control. In *1987 American Control Conference*, pages 1021–1026.
- Chapaloglou, S., Varagnolo, D., Marra, F., and Tedeschi, E. (2022). Data-informed scenario generation for statistically stable energy storage sizing in isolated power systems. *Journal of Energy Storage*, 51:104311.
- Charnes, A., Cooper, W. W., and Kortanek, K. (1962). Duality, haar programs, and finite sequence spaces. *Proceedings of the National Academy of Sciences*, 48(5):783–786.

- Chazelle, B. (1993). An optimal convex hull algorithm in any fixed dimension. *Discrete & Computational Geometry*, 10(4):377–409.
- Cramer, E., Mitsos, A., Tempone, R., and Dahmen, M. (2022). Principal component density estimation for scenario generation using normalizing flows. *Data-Centric Engineering*, 3:e7.
- Dantzig, G. B. (1955). Linear Programming under Uncertainty. *Management Science*, 1(3/4):197–206.
- Diehl, M., Houska, B., Stein, O., and Steuermann, P. (2013). A lifting method for generalized semi-infinite programs based on lower level Wolfe duality. *Computational Optimization and Applications*, 54(1):189–210.
- Djelassi, H. (2020). *Diskretisierungsbasierte Algorithmen für die globale Lösung hierarchischer Optimierungsprobleme*. Dissertation, RWTH Aachen University.
- Djelassi, H., Glass, M., and Mitsos, A. (2019). Discretization-based algorithms for generalized semi-infinite and bilevel programs with coupling equality constraints. *Journal of Global Optimization*, 75(2):341–392.
- Djelassi, H. and Mitsos, A. (2021). Global Solution of Semi-infinite Programs with Existence Constraints. *Journal of Optimization Theory and Applications*, 188(3):863–881.
- Djelassi, H., Mitsos, A., and Stein, O. (2021). Recent advances in nonconvex semi-infinite programming: Applications and algorithms. *EURO Journal on Computational Optimization*, 9:100006.
- Domínguez-Muñoz, F., Cejudo-López, J. M., Carrillo-Andrés, A., and Gallardo-Salazar, M. (2011). Selection of typical demand days for CHP optimization. *Energy and Buildings*, 43(11):3036–3043.
- European Commission (2022). JRC Photovoltaic Geographical Information System (PVGIS). https://re.jrc.ec.europa.eu/pvg_tools/en/. Accessed: 2024-11-12.
- Gils, H. C. and Simon, S. (2017). Carbon neutral archipelago – 100% renewable energy supply for the Canary Islands. *Applied Energy*, 188:342–355.
- Gobierno de Canarias (2023a). Anuario Energetico De Canarias 2021. https://www.gobiernodecanarias.org/energia/descargas/SDE/Portal/Publicaciones/AnuarioEnergeticodeCanarias_2021_v2.pdf, Accessed: 2024-11-20.
- Gobierno de Canarias (2023b). Consejería de Transición Ecológica, Lucha contra el Cambio Climático y Planificación Territorial. <https://www.gobiernodecanarias.org/boc/2023/104/009.html>, Accessed: 2024-11-12.

- Gross, R., Heptonstall, P., Leach, M., Anderson, D., Green, T., and Skea, J. (2007). Renewables and the grid: Understanding intermittency. *Proceedings of the Institution of Civil Engineers - Energy*, 160(1):31–41.
- Grossmann, I. E. and Sargent, R. W. H. (1978). Optimum design of chemical plants with uncertain parameters. *AIChE Journal*, 24(6):1021–1028.
- Guerra Vázquez, F., Rückmann, J.-J., Stein, O., and Still, G. (2008). Generalized semi-infinite programming: A tutorial. *Journal of Computational and Applied Mathematics*, 217(2):394–419.
- Gurobi Optimization, LLC (2024). Gurobi optimizer reference manual. <https://www.gurobi.com>.
- Halemane, K. P. and Grossmann, I. E. (1983). Optimal process design under uncertainty. *AIChE Journal*, 29(3):425–433.
- Heptonstall, P. J. and Gross, R. J. K. (2021). A systematic review of the costs and impacts of integrating variable renewables into power grids. *Nature Energy*, 6(1):72–83.
- Hess, D., Wetzel, M., and Cao, K.-K. (2018). Representing node-internal transmission and distribution grids in energy system models. *Renewable Energy*, 119:874–890.
- Hettich, R. and Kortanek, K. O. (1993). Semi-Infinite Programming: Theory, Methods, and Applications. *SIAM Review*, 35(3):380–429.
- Hoffmann, M., Kotzur, L., Stolten, D., and Robinius, M. (2020). A Review on Time Series Aggregation Methods for Energy System Models. *Energies*, 13(3):641.
- Huber, M., Dimkova, D., and Hamacher, T. (2014). Integration of wind and solar power in Europe: Assessment of flexibility requirements. *Energy*, 69:236–246.
- Huld, T., Müller, R., and Gambardella, A. (2012). A new solar radiation database for estimating PV performance in Europe and Africa. *Solar Energy*, 86(6):1803–1815.
- Kannan, R. and Turton, H. (2013). A Long-Term Electricity Dispatch Model with the TIMES Framework. *Environmental Modeling & Assessment*, 18(3):325–343.
- Keles, D., Jochem, P., McKenna, R., Ruppert, M., and Fichtner, W. (2017). Meeting the Modeling Needs of Future Energy Systems. *Energy Technology*, 5(7):1007–1025.
- Kennedy, N., Miao, C., Wu, Q., Wang, Y., Ji, J., and Roskilly, T. (2017). Optimal Hybrid Power System Using Renewables and Hydrogen for an Isolated Island in the UK. *Energy Procedia*, 105:1388–1393.

- Kotzur, L., Markewitz, P., Robinius, M., and Stolten, D. (2018). Impact of different time series aggregation methods on optimal energy system design. *Renewable Energy*, 117:474–487.
- Kramer, M. A. (1991). Nonlinear principal component analysis using autoassociative neural networks. *AIChE Journal*, 37(2):233–243.
- Li, X. and Barton, P. I. (2015). Optimal design and operation of energy systems under uncertainty. *Journal of Process Control*, 30:1–9.
- Lubin, M., Petra, C. G., Anitescu, M., and Zavala, V. (2011). Scalable stochastic optimization of complex energy systems. In *Proceedings of 2011 International Conference for High Performance Computing, Networking, Storage and Analysis*, SC '11, New York, NY, USA. Association for Computing Machinery.
- Ma, T., Yang, H., and Lu, L. (2014). A feasibility study of a stand-alone hybrid solar–wind–battery system for a remote island. *Applied Energy*, 121:149–158.
- Meschede, H., Holzapfel, P., Kadelbach, F., and Hesselbach, J. (2016). Classification of global island regarding the opportunity of using RES. *Applied Energy*, 175:251–258.
- Mitsos, A. and Tsoukalas, A. (2015). Global optimization of generalized semi-infinite programs via restriction of the right hand side. *Journal of Global Optimization*, 61(1):1–17.
- Papoulias, S. A. and Grossmann, I. E. (1983). A structural optimization approach in process synthesis—I: Utility systems. *Computers & Chemical Engineering*, 7(6):695–706.
- Pearson, K. (1901). On lines and planes of closest fit to systems of points in space. *The London, Edinburgh, and Dublin Philosophical Magazine and Journal of Science*, 2(11):559–572.
- Pfenninger, S., Hawkes, A., and Keirstead, J. (2014). Energy systems modeling for twenty-first century energy challenges. *Renewable and Sustainable Energy Reviews*, 33:74–86.
- Poncelet, K., Delarue, E., Six, D., Duerinck, J., and D’haeseleer, W. (2016). Impact of the level of temporal and operational detail in energy-system planning models. *Applied Energy*, 162:631–643.
- Red Eléctrica de España (2024). La Palma - Electricity demand tracking in real time. https://demanda.ree.es/visiona/canarias/la_palma5m/tablas. Accessed: 2024-11-12.
- Reinert, C., Deutz, S., Minten, H., Dörpinghaus, L., von Pfingsten, S., Baumgärtner, N., and Bardow, A. (2020). Environmental Impacts of the Future German Energy System from Integrated Energy Systems Optimization and Life Cycle Assessment. In Pierucci, S., Manenti, F., Bozzano, G. L., and Manca, D.,

- editors, *Computer Aided Chemical Engineering*, volume 48 of *30 European Symposium on Computer Aided Process Engineering*, pages 241–246. Elsevier.
- Ringkjøb, H.-K., Haugan, P. M., and Solbrekke, I. M. (2018). A review of modelling tools for energy and electricity systems with large shares of variable renewables. *Renewable and Sustainable Energy Reviews*, 96:440–459.
- Rückmann, J.-J. and Reemtsen, R., editors (1998). *Semi-Infinite Programming*, volume 25 of *Springer eBook Collection Mathematics and Statistics*. Springer, Boston, MA.
- Scheel, H. and Scholtes, S. (2000). Mathematical Programs with Complementarity Constraints: Stationarity, Optimality, and Sensitivity. *Mathematics of Operations Research*, 25(1):1–22.
- Schütz, T., Hu, X., Fuchs, M., and Müller, D. (2018). Optimal design of decentralized energy conversion systems for smart microgrids using decomposition methods. *Energy*, 156:250–263.
- Seidel, T. and Küfer, K.-H. (2022). An adaptive discretization method solving semi-infinite optimization problems with quadratic rate of convergence. *Optimization*, 71(8):2211–2239.
- Siala, K., de la Rúa, C., Lechón, Y., and Hamacher, T. (2019). Towards a sustainable European energy system: Linking optimization models with multi-regional input-output analysis. *Energy Strategy Reviews*, 26:100391.
- Stein, O. (2003). *Bi-Level Strategies in Semi-infinite Programming*, volume 71 of *Nonconvex Optimization and Its Applications*. Springer Science+Business Media, New York, NY, softcover repr. of the hardcover 1. ed. edition.
- Stein, O. (2012). How to solve a semi-infinite optimization problem. *European Journal of Operational Research*, 223(2):312–320.
- Stuber, M. D. and Barton, P. I. (2015). Semi-Infinite Optimization with Implicit Functions. *Industrial & Engineering Chemistry Research*, 54(1):307–317.
- Teichgraeber, H. and Brandt, A. R. (2019). Clustering methods to find representative periods for the optimization of energy systems: An initial framework and comparison. *Applied Energy*, 239:1283–1293.
- Teichgraeber, H. and Brandt, A. R. (2022). Time-series aggregation for the optimization of energy systems: Goals, challenges, approaches, and opportunities. *Renewable and Sustainable Energy Reviews*, 157:111984.

- Teichgraeber, H., Lindenmeyer, C. P., Baumgärtner, N., Kotzur, L., Stolten, D., Robinius, M., Bardow, A., and Brandt, A. R. (2020). Extreme events in time series aggregation: A case study for optimal residential energy supply systems. *Applied Energy*, 275:115223.
- Voll, P., Klaffke, C., Hennen, M., and Bardow, A. (2013). Automated superstructure-based synthesis and optimization of distributed energy supply systems. *Energy*, 50:374–388.
- Yunt, M., Chachuat, B., Mitsos, A., and Barton, P. I. (2008). Designing man-portable power generation systems for varying power demand. *AIChE Journal*, 54(5):1254–1269.
- Zingler, A., Mitsos, A., Jungen, D., and Djelassi, H. (2023). libDIPS — Discretization-Based Semi-Infinite and Bilevel Programming Solvers. *Optimization Online*, 24914.

Robust Energy System Design via Semi-infinite Programming – Supplementary Materials

Moritz Wedemeyer^{a,b}, Eike Cramer^c, Alexander Mitsos^{d,a,c}, Manuel Dahmen^{a,*}

^a Institute of Climate and Energy Systems, Energy Systems Engineering (ICE-1), Forschungszentrum Jülich GmbH, Jülich 52425, Germany

^b RWTH Aachen University, Aachen 52062, Germany

^c RWTH Aachen University, Process Systems Engineering (AVT.SVT), Aachen 52074, Germany

^d JARA-ENERGY, Jülich 52425, Germany

1 Illustrative Nonconvex Example: ESIP Subproblems

This section complements Section 3 of the main manuscript and provides the subproblems involved in the solution of the mixed-integer linear program (MILP) existence-constrained semi-infinite programming (ESIP) problem. First, we have the lower bounding problem:

$$\begin{aligned}
 & \min_{x_1, x_2, z_{1,u,k}, b_{u,k}} && 2x_1 + x_2 && \text{(MILP LBP)} \\
 & \text{s.t.} && y_{k, \text{disc}} - z_{1,u,k} - x_2 b_{u,k} \leq 0 && \forall k \in \mathcal{K} \\
 & && 0.2x_2 b_{u,k} + z_{1,u,k} - y_{k, \text{disc}} \leq 0 && \forall k \in \mathcal{K} \\
 & && z_{1,u,k} - x_1 \leq 0 && \forall k \in \mathcal{K} \\
 & && x_1, x_2, z_{1,u,k} \in [0, 100] \\
 & && b_{u,k} \in \{0, 1\}
 \end{aligned}$$

The lower bounding problem (MILP LBP) determines a lower bound on the optimal objective value and fixes the capacities for the subsequent solution of the MAXMIN problem that determines whether the identified design is feasible. The discretization set \mathcal{K} , populated by the medial-level problem, comprises the identified extreme scenarios up to this point and ensures that the identified design is robust. x_1 and x_2 are abstract component capacities. $z_{1,u,k}$ is the operational variable of the lower bounding problem. There are $|\mathcal{K}|$ sets of operational variables, one for each discretization point. $b_{u,k}$ are the lower bounding binary variables used to model the minimal part load of Component 2. The discretization parameter

*M. Dahmen, Institute of Climate and Energy Systems, Energy Systems Engineering (ICE-1), Forschungszentrum Jülich GmbH, Jülich 52425, Germany
E-mail: m.dahmen@fz-juelich.de

$y_{k,disc}$ corresponds to the optimal solution in iteration k to the medial-level problem:

$$\begin{aligned}
 & \min_{y, mlpobj, b_m} -mlpobj & (\text{MILP MLP}) \\
 \text{s.t.} \quad & mlpobj - y + z_{1,l,disc} + b_{l,disc}x_2 - 1000b_m \leq 0 \quad \forall l \in \mathcal{N} \\
 & mlpobj - b_{l,disc}0.2x_2 + y - z_{1,l,disc} - 1000(1 - b_m) \leq 0 \quad \forall l \in \mathcal{N} \\
 & y \in [0, 100] \\
 & mlpobj \in [-1000, 1000] \\
 & b_m \in \{0, 1\}
 \end{aligned}$$

The medial-level problem (MILP MLP) determines worst-case demand realizations for given component capacities x_1 and x_2 for a given discretization set \mathcal{N} populated by the lower-level problem. y is the uncertain demand, and $mlpobj$ is a dummy variable introduced by the epigraph reformulation of the medial-level problem (Djelassi, 2020). b_m is a binary variable introduced to reformulate the maximum introduced by moving the lower-level constraints depending on y into the objective. Discretization parameters $z_{1,l,disc}$ and $b_{l,disc}$ correspond to the optimal values of the operational variables and are determined by the lower-level problem:

$$\begin{aligned}
 & \min_{z_{1,u}, b_u, llpobj} llpobj & (\text{MILP LLP}) \\
 \text{s.t.} \quad & y - z_{1,u} - b_u x_2 - llpobj \leq 0 \\
 & 0.2b_u x_2 - y + z_{1,u} - llpobj \leq 0 \\
 & z_{1,u} - x_1 \leq 0 \\
 & z_{1,u} \in [0, 100] \\
 & llpobj \in [-1000, 1000] \\
 & b_u \in \{0, 1\}
 \end{aligned}$$

The lower-level problem (MILP LLP) describes the operational problem for fixed capacities x_1 and x_2 and fixed demand y . The lower-level problem minimizes the constraint violations of the operational problem and determines the discretization points for the medial-level problem (MILP MLP). Operational variables $z_{1,u}$ and b_u are the lower-level operational variables.

2 La Palma Energy System

This section provides further details on the data processing as well as the complete model formulations for the La Palma energy system introduced in Section 4 of the main manuscript.

2.1 Historical Time-Series Data

For the renewable energy resources, we use data for wind speed at 10 m height and global irradiance obtained from the Photovoltaic Geographical Information System (PVGIS) by the European Union (European Commission, 2022; Huld et al., 2012). We chose the northwest of La Palma (28.780° latitude and −17.980° longitude) as the location for the historical data after a visual inspection using PVGIS (European Commission, 2022; Huld et al., 2012) showed both annual average solar irradiance and average wind speed to be highest in the northwest (European Commission, 2022; Davis et al., 2023). PVGIS uses SARA2.1 (Pfeifroth et al., 2019) and ERA5 (Hersbach et al., 2020) as underlying data sets for solar irradiance and wind speed, respectively. The solar panels are assumed to have an optimal orientation, which PVGIS determines for the chosen location.

The PV unit and wind turbine power outputs are modeled using utilization factors $f_{c,s,t}$, which are bounded by capacity factors $c_{cap,solar,s,t}$ calculated during a preprocessing step. For PV power, the solar capacity factor is calculated from the global irradiance according to Sass et al. (2020) as

$$c_{cap,solar,s,t} = \min\left\{\frac{I_{s,t}\eta_{solar}}{P_{solar,nom}}, 1\right\},$$

where $I_{s,t}$ is the global irradiance in kW/m², $\eta_{solar} = 0.19$ is the assumed efficiency of the PV units, and $P_{solar,nom} = 0.171$ kW/m² is the nominal capacity.

The wind capacity factor is calculated from the wind speed at hub height using the power curve of an Enercon E82/2350 wind turbine (Enercon, 2012) as

$$c_{cap,wind,s,t} = \frac{P_{wind,s,t}}{P_{wind,nom}},$$

where $P_{wind,nom} = 2350$ kW is the nominal capacity of a wind turbine. The power output $P_{wind,s,t}$ for a given wind speed at hub height $v_{wind,hub,t}$ in m/s is calculated by linear interpolation of the power output from the power curve data, which is given for wind speeds in 1 m/s increments. We obtain wind speed at hub height from wind speed at 10 m by using the logarithmic wind profile approximation (Oke,

2006)

$$v_{wind,hub} = v_{wind,10m} \frac{\ln(h_{hub}/z_0)}{\ln(10\text{ m}/z_0)},$$

with a hub height h_{hub} of 85 m and a roughness length z_0 of 0.3 m, determined by visual inspection of the roughness length map in PVGIS ([European Commission, 2022](#); [Huld et al., 2012](#)) for the north-west of La Palma ([Davis et al., 2023](#)). The cutout wind speed for the turbine is 25 m/s. At higher wind speeds, the turbine is shut down, and no power is produced.

Demand data is aggregated from the Spanish electricity distribution system operator [Red Eléctrica de España \(2024\)](#). Solar, wind, and demand data covers the time span from 01.01.2013 until 31.12.2019. We follow the processing introduced in Section 2 of the main manuscript to obtain the representative days and the uncertainty bounds. First, z-normalization is applied to each individual quantity, i.e., solar capacity factors, wind capacity factors, and electricity demand ([Teichgraeber and Brandt, 2019](#)). Normalization is performed for the full time-series data, i.e., for each quantity, all values in the historical data are considered at once, as opposed to normalizing each representative period or each time step individually. The normalized time series data for each attribute are then concatenated, and representative days are selected by k-means clustering ([MacQueen et al., 1967](#)) using the scikit-learn package ([Pedregosa et al., 2011](#)). Default settings are used and the random state is fixed to 42 to ensure reproducibility. To accurately approximate the operational costs, an appropriate number of clusters and, thus, representative scenarios must be selected. The elbow method ([Thorndike, 1953](#)), shown in Figure 1, does not clearly indicate a suitable number of representative days. Furthermore, the elbow method has been criticized for its strong dependence on the scaling of the plot axis and spurious results in case of uncorrelated data ([Schubert, 2023](#)). Pragmatically, we choose 15 representative days to achieve a reasonable balance between the computational effort and the accuracy of the load curve approximation (see Figure 2).

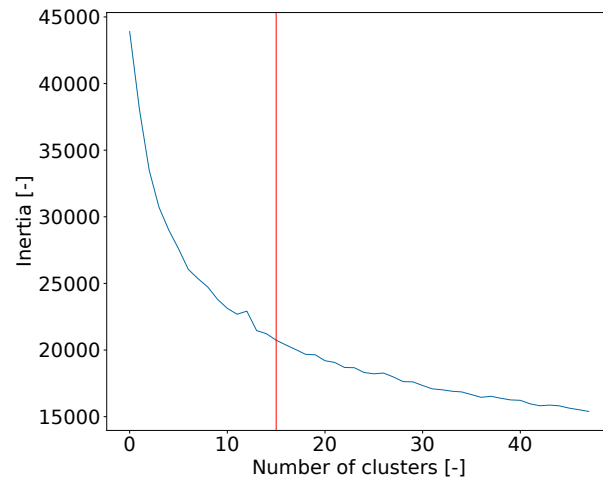


Fig. 1. k-means clustering inertia plotted against the number of clusters (elbow method ([Thorndike, 1953](#))). Clusters are determined using the scikit-learn package ([Pedregosa et al., 2011](#)), default settings are used, and the random state is fixed to 42 to ensure reproducibility. The red line indicates the number of clusters chosen in this study, which is 15.

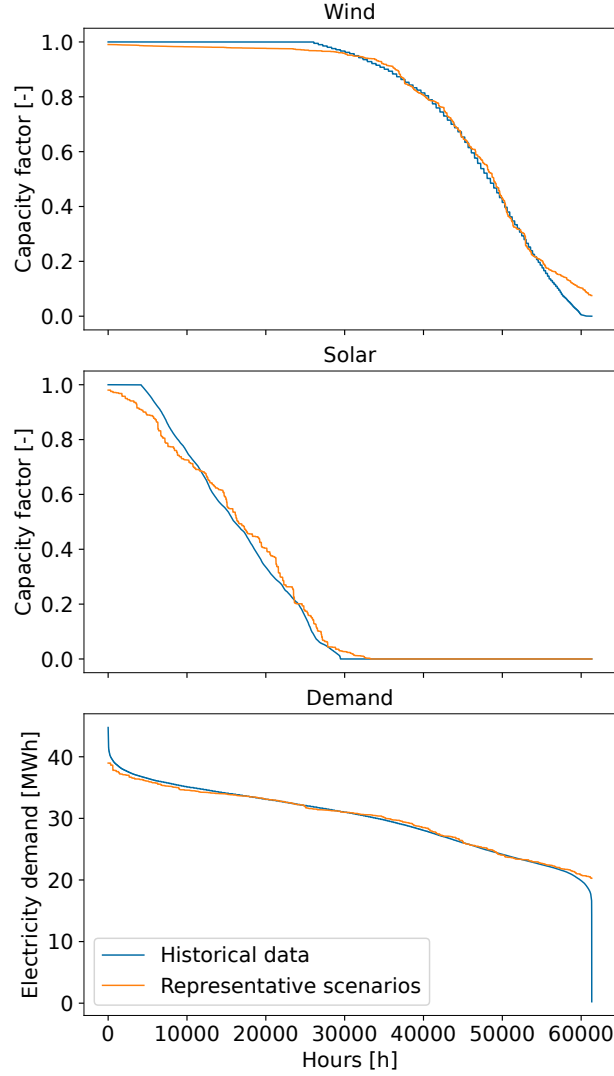


Fig. 2. Load curves (Masters, 2004) for the considered time-series data. Historical data and data of the 15 selected representative days. To compute the load curve for the representative days, we consider the full historical time series but replace each historical day by the corresponding representative day. A good agreement between the load curves of the historical data and the representative scenarios can be seen, indicating that the representative scenarios can approximate the total yearly load well.

To determine the uncertainty bounds, we reduce the dimensionality of the concatenated time-series data using principal component analysis (PCA) (Pearson, 1901) implemented in scikit-learn (Pedregosa et al., 2011). We use 'full' for the `svd_solver` parameter to calculate the exact PCA decomposition and default values for all remaining parameters. Then, we determine the convex hull, using the SciPy package (Virtanen et al., 2020) on the latent space historical data.

Component c	$c_{inv,c}$ in € ₂₀₂₂ /kW	$c_{fix,c}$ in € ₂₀₂₂ /kW	$c_{var,c}$ in € ₂₀₂₂ /kWh
Solar	883.3	17.9	0
Wind	2283.7	26.9	0.011
Diesel	2391.8	0	0.242
Battery	1550	31	0

Tab. 1. Cost parameters of the considered components.

2.2 Model Formulation

For ease of notation, we define the set of generation components $\mathcal{C} = \{solar, wind, diesel\}$. Similar to [Sass et al. \(2020\)](#), we use total annualized cost (TAC) as our objective, i.e.,

$$\begin{aligned} \min_{\mathbf{x} \in \mathcal{X}, \mathbf{z}_s \in \mathcal{Z}_s} \quad & \sum_{c \in \mathcal{C} \cup \{battery\}} P_{c,peak} \left(\frac{c_{inv,c}}{f_{AN}} + c_{fix,c} \right) \\ & + 365 \sum_{s \in \mathcal{S}} \omega_s \sum_{c \in \mathcal{C}} \sum_{t \in \mathcal{T}} \Delta_t P_{c,peak} f_{c,s,t} c_{var,c}, \end{aligned}$$

with design decisions \mathbf{x} and operational variables \mathbf{z}_s . The objective function consists of investment costs for each generation component and the battery c , calculated by multiplying its installed capacity $P_{c,peak}$ with the specific investment costs $c_{inv,c}$. Similarly, fixed operational costs $c_{fix,c}$ are considered for each year of operation. Additionally, investment costs are divided by the present value annuity factor

$$f_{AN} = \frac{(1+i)^T - 1}{i(1+i)^T},$$

which is determined with an assumed interest rate i of 8% and a time horizon T of 25 years. Finally, variable operational costs $c_{var,c}$ are multiplied by the provided amount of electricity by each generation component in each time step t for every representative scenario s . To this end, the length of each time step Δ_t is multiplied by the installed capacity and the capacity factor $f_{c,s,t}$. The cost for each representative scenario are then weighted by ω_s , the number of days in each cluster $n_{days,s}$ divided by the number of total days n_{days} , see e.g., [Nahmmacher et al. \(2016\)](#), i.e.,

$$\omega_s = \frac{n_{days,s}}{n_{days}}.$$

Yearly variable operational costs are calculated by scaling the costs of the representative days to a year. Table 1 summarizes all cost parameters used in this study. We adjusted all costs to a 2022 base using the EU domestic producer price index for the 19-country Euro area ([eurostat, 2024](#)). Details on how the cost parameters are obtained and adjusted for inflation are given in Section 2.3.

We introduce a constraint to ensure that the power demand is satisfied for every time step in every scenario:

$$P_{demand,s,t} + P_{battery,in,s,t} - P_{battery,out,s,t} - \sum_{c \in \mathcal{C}} P_{c,peak} f_{c,s,t} \leq 0 \quad \forall s \in \mathcal{S} \quad \forall t \in \mathcal{T}$$

$P_{demand,s,t}$ is the electricity demand at time step t of a representative day s . Equation $f_{c,s,t} - c_{cap,c,s,t} \leq 0$ describes that capacity factors $f_{c,s,t}$ have to be less than the capacity factor parameters for the representative scenarios $c_{cap,c,s,t}$. For the diesel generator the capacity factor parameters are 1, i.e., $c_{cap,diesel,s,t} = 1$.

The battery system is modeled following [Sass et al. \(2020\)](#). Separate variables $P_{battery,in,s,t}$ and $P_{battery,out,s,t}$ are introduced for charging and discharging to account for charging and discharging losses. The relation between peak power output $P_{battery,peak}$ and peak capacity $E_{battery,peak}$ is assumed to be 4 kWh/kW, i.e., a constraint $E_{battery,peak} = 4P_{battery,peak}$ is added. The change in the stored electricity E is described by

$$\frac{dE}{dt} = \frac{1}{3600}(\eta_{in}P_{battery,in} + \frac{1}{\eta_{out}}P_{battery,out}),$$

with charging efficiency $\eta_{in} = 0.92$ and discharging efficiency $\eta_{out} = 0.926$ based on [Baumgärtner et al. \(2019\)](#). We discretize the differential equation using the forward Euler scheme ([Euler, 2000](#)), i.e., we obtain

$$\begin{aligned} \dot{E}_{battery,s,t} - \frac{1}{3600}(\eta_{in}P_{battery,in,s,t} + \frac{1}{\eta_{out}}P_{battery,out,s,t}) &= 0 \quad \forall s \in \mathcal{S} \quad \forall t \in \mathcal{T}, \\ \dot{E}_{battery,s,t}\Delta t - (E_{battery,s,t} - E_{battery,s,t-1}) &= 0 \quad \forall s \in \mathcal{S} \quad \forall t \in \mathcal{T}, \end{aligned}$$

where Δt is the time step length, $E_{bat,s,t}$ is the state of charge, and $\dot{E}_{bat,s,t}$ the rate of charge. The initial state of charge is assumed to be 50 % of the nominal capacity. Additionally, there is a cyclical constraint requiring that the battery is recharged to the initial level at the end of the representative period.

We model the diesel generator as a dispatchable electricity source, with power output calculated from installed capacity $P_{diesel,peak}$ and variable utilization factor $f_{diesel,s,t}$. We assume that ramping constraints for the diesel generator can be neglected for the investigated temporal resolution. Furthermore, we assume that no minimal part load is needed since the installed diesel generators consist of multiple engines whose individual part loads are small compared to the overall load.

An embedded optimization problem is added that guarantees the feasibility of the design for the

worst-case uncertainty realization:

$$\max_{\mathbf{y} \in \mathcal{Y}(\mathbf{x})} \min_{\mathbf{z} \in \mathcal{Z}_{epi}(\mathbf{x}, \mathbf{y})} \max_{t \in \mathcal{T}} P_{demand,wc,t} + P_{battery,in,wc,t} - P_{battery,out,wc,t} - \sum_{c \in \mathcal{C}} P_{c,peak} f_{c,wc,t} \leq 0$$

Its objective is to maximize the electricity supply gap by searching for the worst-case renewable capacity factors $f_{wind,wc,t}$, $f_{solar,wc,t}$, and demand realizations $P_{demand,wc,t}$. To compensate for the worst-case realization, the battery operation, i.e., $P_{battery,in,wc,t}$ and $P_{battery,out,wc,t}$, as well as the diesel engine utilization factor $f_{diesel,wc,t}$ can be adjusted. Notice that the utilization factor for the diesel engine $f_{diesel,wc,t}$ can be chosen freely within the interval $[0, 1]$ since it does not appear in any of the lower-level constraints. It has a negative sign in the objective function of the embedded minimization problem, so an optimal solution exists where it is at its upper bound 1. Thus, we fix $f_{diesel,wc,t} = 1$ to reduce the computational complexity.

We use PCA to reduce the dimensionality of the optimization problem to facilitate computational tractability. To this end, we calculate the worst-case demand $P_{demand,wc,t}$, as well as the worst-case wind and solar capacity factors $f_{wind,wc,t}$ and $f_{solar,wc,t}$ from principal component factors p_{dim} , which are optimization variables of the embedded maximization problem. Worst-case demand is calculated according to

$$c_{pca,demand,0,t} + \sum_{dim=1}^{n_{dim}} c_{pca,demand,dim,t} p_{dim} - P_{demand,wc,t} = 0 \quad \forall t \in \mathcal{T}$$

$c_{pca,demand,0,t}$ is the mean of the historical demand data, and $c_{pca,demand,dim,t}$ are the principal components that are parameters in the optimization problem and computed during preprocessing using the scikit-learn package (Pedregosa et al., 2011). There are n_{dim} principal components where n_{dim} is the number of dimensions of the latent space. Similarly, we compute worst-case wind and solar capacity factors according to

$$c_{pca,c,0,t} + \sum_{dim=1}^{n_{dim}} c_{pca,c,dim,t} p_{dim} - f_{c,wc,t} \leq 0 \quad \forall c \in \{solar, wind\} \quad \forall t \in \mathcal{T},$$

where we additionally introduce the equation

$$-f_{c,wc,t} \leq 0 \quad \forall c \in \{solar, wind\} \quad \forall t \in \mathcal{T}$$

to ensure that negative capacity factors due to PCA truncation errors do not occur.

Finally, we provide the equations for the convex hull. There are two equivalent formulations of the convex hull around the historical data in the principal component space (Avis et al., 1997). First, the

convex hull can be encoded by an intersection of halfspaces as

$$\sum_{dim=1}^{n_{dim}} a_{dim,j} p_{dim} + b_{conv,j} \leq 0 \quad \forall j \in \mathcal{J},$$

where $a_{dim,j}$ and $b_{conv,j}$ are parameters describing the hyperplanes bounding the historical data. $a_{dim,j}$ and $b_{conv,j}$ are obtained using the 'ConvexHull' function of the SciPy package (Virtanen et al., 2020).

Second, the convex hull can be described as a linear combination of its vertices, i.e.,

$$\sum_{v=1}^{n_v} \alpha_v c_{data,v,dim} = p_{dim} \quad \forall dim \in \{1, \dots, n_{dim}\},$$

where $c_{data,v,dim}$ is the dim -th component of the latent representation vector $\mathbf{c}_{data,v}$ of the vertex v and α_v are the factors describing the weights of the vertices with the restriction

$$\sum_{v=1}^{n_v} \alpha_v = 1.$$

The vertices are again obtained using the 'ConvexHull' function of the SciPy package (Virtanen et al., 2020). In preliminary studies, we found that representing the uncertainty set in the optimization problem as a convex combination of the vertices yielded the best computational performance in our case study. Hence, we formulate the convex hull as a convex combination of its vertices in all our numerical experiments.

2.3 Cost Parameters

We adjust all price data for inflation to bring them to a 2022 base. To this end, we calculate an average annual producer price index (eurostat, 2024) ppi_{yr} from monthly data $ppi_{yr,mon}$:

$$ppi_{yr} = \frac{1}{12} \sum_{mon=1}^{12} ppi_{yr,mon}$$

The adjusted price pr_{2022} in €_{2022} is then calculated from the price pr_{yr} for the reference year yr and the corresponding average annual producer price indices:

$$pr_{2022} = pr_{yr} \frac{ppi_{2022}}{ppi_{yr}}$$

Investment and operational costs for wind and solar are obtained from Kost et al. (2021). Specifically, we use the center of the provided intervals for onshore wind and utility-scale PV data. Battery investment

costs are taken as the center of the interval given by [Figgenger et al. \(2023\)](#) for large-scale energy storage and multiplied by the assumed energy storage ratio of 4 kWh/kW to obtain the battery capacity in kW, which is the unit of the battery capacity (see Section 2.2). Operational costs are assumed to be 2% of investment costs following [Kost et al. \(2021\)](#). Investment costs and variable costs of the diesel generators are calculated according to information from Spanish legislation ([Ministerio de Industria, Energía y Turismo, 2015](#)). To calculate diesel generator cost, we assume the use of 11.5 MW four-stroke diesel engines, as this is the size of the diesel generators most recently added to the island generation park ([Ministerio de Industria, Energía y Turismo, 2015](#)). Variable costs are calculated according to Spanish legislation ([Ministerio de Industria, Energía y Turismo, 2015](#)):

$$c_{diesel,var} = co_{fuel} + co_{start-up} + co_{maintenance} + co_{dispatch} + co_{CO2} + co_{reduction}$$

Variable fuel costs $co_{fuel} = 0.12 \text{ €}_{2022}/\text{kWh}$ were calculated from data released by Spanish ministerial orders:

$$co_{fuel} = \frac{pr_{fuel} + pr_{logistics}}{LHV \eta_{therm}}$$

Here, we assumed a fuel price for 1% fuel oil in the Canaries of $448.38 \text{ €}_{2022}/\text{t}$, which is the average over the first 6 months of 2023 ([Ministerio para la Transición Ecológica y el Reto Demográfico, 2023b](#)) and logistic costs for transport to La Palma of $103.47 \text{ €}_{2022}/\text{t}$ ([Ministerio para la Transición Ecológica y el Reto Demográfico, 2022](#)). The lower heating value for the 1% fuel oil is taken as $11\,214.46 \text{ kWh/t}$ ([Ministerio para la Transición Ecológica y el Reto Demográfico, 2023a](#)) and we use the average thermal efficiency of the currently used diesel generators $\eta_{therm} = 0.41$ ([Gobierno de Canarias, 2023](#)). We neglect the dispatch start-up costs $co_{start-up}$ as we model the diesel generators in a simplified way without minimum part load constraints. We assume the variable maintenance costs as $0.042 \text{ €}_{2022}/\text{kWh}$, identical to the current 11.5 MW four-stroke diesel engines ([Ministerio de Industria, Energía y Turismo, 2015](#)). Dispatch regulation band costs $co_{dispatch}$ are 1% of the sum of variable fuel costs and costs of dispatch emission rights. Costs of dispatch emission rights $co_{CO2} = 0.079 \text{ €}_{2022}/\text{kWh}$ are calculated according to ([Ministerio de Industria, Energía y Turismo, 2015](#)):

$$co_{CO2} = pr_{CO2L} fa_{emission} co_{corr,p} co_{corr,e}$$

Here, the price of dispatch allowances pr_{CO2L} is $80.821 \text{ €}_{2022}/\text{t}$ ([Ministerio para la Transición Ecológica y el Reto Demográfico, 2023c](#)), the emission factor $fa_{emission}$ is $0.62 \text{ t}_{CO2}/\text{MWh}$ ([Ministerio de la Presiden-](#)

cia, 2006), the correlation factor $co_{corr,p}$ is 1.028. Pragmatically, we assume the correlation factor $co_{corr,e}$ as 1 since no values have been published by the responsible ministry yet. Furthermore, the reduction of variable costs due to income or avoided costs unrelated to electricity production $co_{reduction}$ is neglected.

2.4 Problem Formulation

In this Section, we provide the full problem formulation for the La Palma robust energy system design (see Section 4 in the main manuscript).

$$\begin{aligned}
& \min_{\mathbf{x} \in \mathbb{R}_{\geq 0}^{|\mathcal{C}|+2}, \mathbf{z}_s \in \mathbb{R}^{|\mathcal{S}||\mathcal{T}|(|\mathcal{C}|+4)}} \sum_{c \in \mathcal{C} \cup \{\text{battery}\}} P_{c,peak} \left(\frac{c_{inv,c}}{f_{AN}} + c_{fix,c} \right) \quad (\text{Full Design Problem}) \\
& + 365 \sum_{s \in \mathcal{S}} \omega_s \sum_{c \in \mathcal{C}} \sum_{t \in \mathcal{T}} \Delta_t P_{c,peak} f_{c,s,t} c_{var,c}, \\
& \text{s.t.} \quad P_{demand,s,t} + P_{battery,in,s,t} - P_{battery,out,s,t} - \sum_{c \in \mathcal{C}} P_{c,peak} f_{c,s,t} \leq 0 \quad \forall s \in \mathcal{S} \quad \forall t \in \mathcal{T}, \\
& \quad - f_{c,s,t} \leq 0 \quad \forall c \in \mathcal{C} \quad \forall s \in \mathcal{S} \quad \forall t \in \mathcal{T}, \\
& \quad f_{diesel,s,t} - 1 \leq 0 \quad \forall s \in \mathcal{S} \quad \forall t \in \mathcal{T}, \\
& \quad f_{c,s,t} - c_{cap,c,s,t} \leq 0 \quad \forall c \in \{\text{wind}, \text{solar}\} \quad \forall s \in \mathcal{S} \quad \forall t \in \mathcal{T}, \\
& \quad P_{battery,out,s,t} - P_{battery,peak} \leq 0 \quad \forall s \in \mathcal{S} \quad \forall t \in \mathcal{T}, \\
& \quad - P_{battery,in,s,t} \leq 0 \quad \forall s \in \mathcal{S} \quad \forall t \in \mathcal{T}, \\
& \quad P_{battery,in,s,t} - P_{battery,peak} \leq 0 \quad \forall s \in \mathcal{S} \quad \forall t \in \mathcal{T}, \\
& \quad - P_{battery,out,s,t} \leq 0 \quad \forall s \in \mathcal{S} \quad \forall t \in \mathcal{T}, \\
& \quad E_{battery,s,t} - E_{battery,peak} \leq 0 \quad \forall s \in \mathcal{S} \quad \forall t \in \mathcal{T}, \\
& \quad - E_{battery,s,t} \leq 0 \quad \forall s \in \mathcal{S} \quad \forall t \in \mathcal{T}, \\
& \quad \dot{E}_{battery,s,t} - \frac{1}{3600} (\eta_{in} P_{battery,in,s,t} - \frac{1}{\eta_{out}} P_{battery,out,s,t}) = 0 \quad \forall s \in \mathcal{S} \quad \forall t \in \mathcal{T}, \\
& \quad \dot{E}_{battery,s,t} \Delta t - (E_{battery,s,t} - E_{battery,s,t-1}) = 0 \quad \forall s \in \mathcal{S} \quad \forall t \in \mathcal{T}, \\
& \quad E_{battery,s,0} - 0.5 E_{battery,peak} = 0 \quad \forall s \in \mathcal{S}, \\
& \quad E_{battery,peak} - 4 P_{battery,peak} = 0, \\
& \quad \max_{\mathbf{y} \in \mathcal{Y}} \min_{\mathbf{z} \in \mathcal{Z}_{epi}(\mathbf{x}, \mathbf{y})} e_{epi} \leq 0,
\end{aligned}$$

with

$$\begin{aligned}
\mathbf{x} &= [P_{1,peak}, \dots, P_{\mathcal{C}|,peak}, P_{battery,peak}, E_{battery,peak}] \\
\mathbf{z}_s &= [P_{battery,in,1,1}, \dots, P_{battery,in,1,|\mathcal{T}|}, P_{battery,in,2,1}, \dots, P_{battery,in,|\mathcal{S}|,|\mathcal{T}|}, P_{battery,out,1,1}, \dots, P_{battery,out,1,|\mathcal{T}|}, \\
&\quad P_{battery,out,2,1}, \dots, P_{battery,out,|\mathcal{S}|,|\mathcal{T}|}, E_{battery,1,1}, \dots, E_{battery,1,|\mathcal{T}|}, E_{battery,2,1}, \dots, E_{battery,|\mathcal{S}|,|\mathcal{T}|}, \dot{E}_{battery,1,1}, \dots, \\
&\quad \dot{E}_{battery,1,|\mathcal{T}|}, \dot{E}_{battery,2,1}, \dots, \dot{E}_{battery,|\mathcal{S}|,|\mathcal{T}|}, f_{1,1,1}, \dots, f_{1,1,|\mathcal{T}|}, f_{1,2,1}, \dots, f_{1,|\mathcal{S}|,|\mathcal{T}|}, f_{2,1,1}, \dots, f_{\mathcal{C}|,|\mathcal{S}|,|\mathcal{T}|}] \\
\mathbf{y} &= [f_{wind,wc,1}, \dots, f_{wind,wc,|\mathcal{T}|}, f_{solar,wc,1}, \dots, f_{solar,wc,|\mathcal{T}|}, p_1, \dots, p_{|n_{dim}|}, P_{demand,wc,1}, \dots, P_{demand,wc,|\mathcal{T}|}, \\
&\quad \alpha_1, \dots, \alpha_{|n_v|}] \\
\mathcal{Y} &= \{\mathbf{y} \in \mathbb{R}^{3|\mathcal{T}|+|n_v|+|n_{dim}|} \mid \mathbf{g}_{\mathbf{y}}(\mathbf{y}) \leq \mathbf{0} \wedge \mathbf{h}_{\mathbf{y}}(\mathbf{y}) = \mathbf{0}\}, \\
\mathbf{g}_{\mathbf{y}}(\mathbf{y}) : \\
&\quad c_{pca,c,0,t} + \sum_{dim=1}^{n_{dim}} c_{pca,c,dim,t} p_{dim} - f_{c,wc,t} \leq 0 \quad \forall c \in \{solar, wind\} \quad \forall t \in \mathcal{T}, \\
&\quad -f_{c,wc,t} \leq 0 \quad \forall c \in \{solar, wind\} \quad \forall t \in \mathcal{T}. \\
\mathbf{h}_{\mathbf{y}}(\mathbf{y}) : \\
&\quad c_{pca,c,0,t} + \sum_{dim=1}^{n_{dim}} c_{pca,c,dim,t} p_{dim} - P_{demand,wc,t} = 0 \quad \forall c \in \{demand\} \quad \forall t \in \mathcal{T}, \\
&\quad \sum_{v=1}^{n_v} \alpha_v c_{data,v,dim} = p_{dim} \quad \forall dim \in \{1, \dots, n_{dim}\}, \\
&\quad \sum_{v=1}^{n_v} \alpha_v = 1. \\
\mathbf{z} &= [P_{battery,in,wc,1}, \dots, P_{battery,in,wc,|\mathcal{T}|}, P_{battery,out,wc,1}, \dots, P_{battery,out,wc,|\mathcal{T}|}, E_{battery,wc,1}, \dots, E_{battery,wc,|\mathcal{T}|}, \\
&\quad \dot{E}_{battery,wc,1}, \dots, \dot{E}_{battery,wc,|\mathcal{T}|}, f_{diesel,wc,1}, \dots, f_{diesel,wc,|\mathcal{T}|,e_{epi}}] \\
\mathcal{Z}_{epi}(\mathbf{x}, \mathbf{y}) &= \{\mathbf{z} \in \mathbb{R}^{5|\mathcal{T}|+1} \mid \mathbf{g}_{\mathbf{z}}(\mathbf{x}, \mathbf{z}) \leq \mathbf{0} \wedge \mathbf{h}_{\mathbf{z}}(\mathbf{x}, \mathbf{z}) = \mathbf{0} \wedge \\
&\quad P_{demand,wc,t} + P_{battery,in,wc,t} - P_{battery,out,wc,t} - \sum_{c \in \mathcal{C}} P_{c,peak} f_{c,wc,t} - e_{epi} \leq 0 \quad \forall t \in \mathcal{T}\} \\
\mathbf{g}_{\mathbf{z}}(\mathbf{x}, \mathbf{z}) : \\
&\quad P_{battery,out,s,t} - P_{battery,peak} \leq 0 \quad \forall t \in \mathcal{T}, \\
&\quad -P_{battery,in,s,t} \leq 0 \quad \forall t \in \mathcal{T}, \\
&\quad P_{battery,in,s,t} - P_{battery,peak} \leq 0 \quad \forall t \in \mathcal{T}, \\
&\quad -P_{battery,out,s,t} \leq 0 \quad \forall t \in \mathcal{T}, \\
&\quad E_{battery,s,t} - E_{battery,peak} \leq 0 \quad \forall t \in \mathcal{T},
\end{aligned}$$

$$-E_{battery,s,t} \leq 0 \quad \forall t \in \mathcal{T}.$$

$$\mathbf{h}_{\mathbf{z}}(\mathbf{x}, \mathbf{z}) :$$

$$\dot{E}_{battery,wc,t} - \frac{1}{3600}(\eta_{in}P_{battery,in,wc,t} - \frac{1}{\eta_{out}}P_{battery,out,wc,s,t}) = 0 \quad \forall t \in \mathcal{T},$$

$$E_{battery,s,0} - 0.5E_{battery,peak} = 0,$$

$$\dot{E}_{battery,s,t}\Delta t - (E_{battery,s,t} - E_{battery,s,t-1}) = 0 \quad \forall t \in \mathcal{T},$$

$$f_{diesel,wc,t} - 1 = 0 \quad \forall t \in \mathcal{T}.$$

Explanations for all symbols were introduced in Sections 2.2 and 2.3. Note the presence of a coupling equality constraint, i.e., $E_{battery,s,0} - 0.5E_{battery,peak} = 0$, which we did not remove since no convergence issues occurred. Furthermore, note the independence of the energy system model equations $\mathbf{g}_{\mathbf{z}}(\mathbf{x}, \mathbf{z})$ and $\mathbf{h}_{\mathbf{z}}(\mathbf{x}, \mathbf{z})$ of \mathbf{y} .

2.5 Lifted Problem Formulation

We apply the lifting approach described in Section 3 of the main manuscript to transform the MAXMIN problem into a single-level NLP.

$$\begin{aligned} \max_{\mathbf{y}, \mathbf{z}, \boldsymbol{\lambda}, \boldsymbol{\mu}} \quad & \mathcal{L}_{ll}(\mathbf{x}, \mathbf{y}, \mathbf{z}, \boldsymbol{\lambda}, \boldsymbol{\mu}), \\ \text{s.t.} \quad & \nabla_{\mathbf{z}} \mathcal{L}_{ll}(\mathbf{x}, \mathbf{y}, \mathbf{z}, \boldsymbol{\lambda}, \boldsymbol{\mu}) = \mathbf{0}, \\ & \boldsymbol{\mu} \geq \mathbf{0}, \\ & \boldsymbol{\mu}^\top \mathbf{g}_{\mathbf{z}}(\mathbf{x}, \mathbf{y}, \mathbf{z}) = \mathbf{0}, \\ & \mathbf{g}_{\mathbf{z}}(\mathbf{x}, \mathbf{y}, \mathbf{z}) \leq \mathbf{0}, \\ & \mathbf{h}_{\mathbf{z}}(\mathbf{x}, \mathbf{z}) = \mathbf{0}, \\ & c_{pca,c,0,t} + \sum_{dim=1}^{n_{dim}} c_{pca,c,dim,t} p_{dim} - f_{c,wc,t} \leq 0 \quad \forall c \in \{solar, wind\} \quad \forall t \in \mathcal{T}, \\ & -f_{c,wc,t} \leq 0 \quad \forall c \in \{solar, wind\} \quad \forall t \in \mathcal{T}, \\ & c_{pca,c,0,t} + \sum_{dim=1}^{n_{dim}} c_{pca,c,dim,t} p_{dim} - P_{demand,wc,t} = 0 \quad \forall c \in \{demand\} \quad \forall t \in \mathcal{T}, \\ & \sum_{v=1}^{n_v} \alpha_v c_{data,v,dim} = p_{dim} \quad \forall dim \in \{1, \dots, n_{dim}\}, \end{aligned}$$

$$\sum_{v=1}^{n_v} \alpha_v = 1,$$

with

$$\begin{aligned} \mathbf{y} &= [f_{wind,wc,1}, \dots, f_{wind,wc,|\mathcal{T}|}, f_{solar,wc,1}, \dots, f_{solar,wc,|\mathcal{T}|}, p_1, \dots, p_{|n_{dim}|}, P_{demand,wc,1}, \dots, P_{demand,wc,|\mathcal{T}|}, \\ &\alpha_1, \dots, \alpha_{|n_v|}] \in \mathbb{R}^{3|\mathcal{T}|+|n_v|+|n_{dim}|}, \\ \mathbf{z} &= [P_{battery,in,wc,1}, \dots, P_{battery,in,wc,|\mathcal{T}|}, P_{battery,out,wc,1}, \dots, P_{battery,out,wc,|\mathcal{T}|}, E_{battery,wc,1}, \dots, E_{battery,wc,|\mathcal{T}|}, \\ &\dot{E}_{battery,wc,1}, \dots, \dot{E}_{battery,wc,|\mathcal{T}|}, f_{diesel,wc,1}, \dots, f_{diesel,wc,|\mathcal{T}|,e_{epi}}] \in \mathbb{R}^{5|\mathcal{T}|+1} \\ \boldsymbol{\lambda} &\in \mathbb{R}^{3|\mathcal{T}|+1}, \\ \boldsymbol{\mu} &\in \mathbb{R}^{7|\mathcal{T}|}, \\ \mathbf{g}_{\mathbf{z}}(\mathbf{x}, \mathbf{y}, \mathbf{z}) : \\ &P_{demand,wc,t} + P_{battery,in,wc,t} - P_{battery,out,wc,t} - \sum_{c \in \mathcal{C}} P_{c,peak} f_{c,wc,t} - e_{epi} \leq 0 \quad \forall t \in \mathcal{T}, \\ &P_{battery,out,wc,s,t} - P_{battery,peak} \leq 0 \quad \forall t \in \mathcal{T}, \\ &-P_{battery,in,wc,s,t} \leq 0 \quad \forall t \in \mathcal{T}, \\ &P_{battery,in,wc,s,t} - P_{battery,peak} \leq 0 \quad \forall t \in \mathcal{T}, \\ &-P_{battery,out,wc,s,t} \leq 0 \quad \forall t \in \mathcal{T}, \\ &E_{battery,wc,s,t} - E_{battery,peak} \leq 0 \quad \forall t \in \mathcal{T}, \\ &-E_{battery,wc,s,t} \leq 0 \quad \forall t \in \mathcal{T}. \\ \mathbf{h}_{\mathbf{z}}(\mathbf{x}, \mathbf{z}) : \\ &\dot{E}_{battery,wc,t} - \frac{1}{3600}(\eta_{in} P_{battery,in,wc,t} - \frac{1}{\eta_{out}} P_{battery,out,wc,s,t}) = 0 \quad \forall t \in \mathcal{T}, \\ &E_{battery,wc,s,0} - 0.5 E_{battery,peak} = 0, \\ &\dot{E}_{battery,wc,s,t} \Delta t - (E_{battery,wc,s,t} - E_{battery,wc,s,t-1}) = 0 \quad \forall t \in \mathcal{T}, \\ &f_{diesel,wc,t} - 1 = 0 \quad \forall t \in \mathcal{T}. \\ \mathcal{L}_l(\mathbf{x}, \mathbf{y}, \mathbf{z}, \boldsymbol{\lambda}, \boldsymbol{\mu}) &= e_{epi} + \boldsymbol{\lambda}^\top \mathbf{h}_{\mathbf{z}}(\mathbf{x}, \mathbf{z}) + \boldsymbol{\mu}^\top \mathbf{g}_{\mathbf{z}}(\mathbf{x}, \mathbf{y}, \mathbf{z}) \end{aligned}$$

Where \mathcal{L}_l is the Lagrangian function and $\boldsymbol{\mu}$ and $\boldsymbol{\lambda}$ are the Lagrange multipliers for the inequalities and equalities, respectively. Explanations for all remaining symbols were introduced in Sections 2.2 and 2.3.

3 Solver Settings

We describe the libDIPS (Zingler et al., 2023) settings as well as the Gurobi (version 11.0.3) (Gurobi Optimization, LLC, 2024) settings that we used to generate the results shown in Section 3 and 4 of the main manuscript. libDIPS was used for the solution of hierarchical programs and Gurobi was used to solve the problems formulated by libDIPS. Table 2 shows the settings that deviate from the default

Name	Value
sip_bnf_demo.cpp	
feas_tol	5×10^{-2}
abs_tol_lbp	5×10^{-3}
rel_tol_lbp	5×10^{-3}
abs_tol_lbp_llp	1×10^{-2}
rel_tol_lbp_llp	5×10^{-3}
max_time	10 800
esip_bnf_demo.cpp	
feas_tol	5×10^{-2}
esip_bnf_solver.hpp	
abs_tol	1×10^{-2}
rel_tol	2×10^{-1}
abs_tol_minmax	2.5×10^{-2}
rel_tol_minmax	1×10^{-3}
Gurobi_solver.hpp	
non_convex	2
num_threads	4
OBBT	3
Presolve	2
FuncNonlinear	1

Tab. 2. libDIPS (Zingler et al., 2023) settings.

settings of libDIPS and Gurobi. If not otherwise stated, the default values were used. The filenames refer to the files where these settings were changed, e.g., 'sip_bnf_demo.cpp'.

The libDIPS parameters that were changed to solve the SIP problem are: 'feas_tol' is the feasibility tolerance of the semi-infinite constraint for which the problem is considered feasible. 'abs_tol_lbp', 'abs_tol_llp', 'rel_tol_lbp', and 'rel_tol_llp' are the absolute and relative optimality tolerances for the lower bounding and lower-level problems, respectively. 'max_time' is the maximum wall-clock time before the optimization is aborted if convergence is not reached.

The libDIPS parameters that were changed to solve the ESIP problem are: 'feas_tol' is the feasibility tolerance of the semi-infinite existence constraint for which the problem is considered feasible. 'abs_tol', and 'rel_tol' are the absolute and relative optimality tolerances for the lower bounding problem. 'abs_tol_minmax', and 'rel_tol_minmax' are the absolute and relative optimality tolerances for

the min-max implementation in libDIPS and are multiplied with respective factors in the code to provide tolerances for the medial- and lower-level problems.

Finally, the altered parameters specific to the Gurobi ([Gurobi Optimization, LLC, 2024](#)) solver are given: 'non_convex' enables Gurobi to handle nonconvex problems. 'num_threads' informs Gurobi about the number of threads to use in parallel to solve the optimization problem. 'OBBT' sets the amount of work allowed for optimality-based bound tightening, 3 is the most aggressive setting. 'Presolve' sets the presolve level, 2 is aggressive presolving, taking more time but yielding a tighter model. 'FuncNon-linear' determines how nonlinear equations are handled. 1 approximates nonlinear equations by outer approximation.

Nomenclature

This Section extends the Nomenclature of the main manuscript. Throughout the manuscript, scalar-valued quantities are denoted in regular font, e.g., x , vector-valued quantities are denoted in bold font, e.g., \mathbf{x} , and set-valued quantities are denoted in calligraphic font, e.g., \mathcal{X} .

Abbreviations

ESIP	existence-constrained semi-infinite program
MILP	mixed-integer linear program
MW	megawatt
NLP	nonlinear program
LHV	lower heating value
RESD	robust energy system design
PC	principal component
PCA	principal component analysis
PV	photo voltaic
SIP	semi-infinite program
TAC	total annualized cost

Greek Symbols

α	weighting factor
Δ_t	time-step length
η	efficiency factor
λ	Lagrange multipliers for equality constraints
μ	Lagrange multipliers for inequality constraints
ω_s	weighting factor for representative scenarios

Latin Symbols

a	factor in convex hull equation
b_{ll}	lower-level binary variable for on/off decision
b_{conv}	factor in convex hull equation
b_u	upper-level binary variable for on/off decision
b_m	medial-level binary variable to reformulate the maximum in the objective function
c_{cap}	capacity factor parameter
c_{fix}	fixed costs
c_{inv}	investment costs
c_{pca}	principal component analysis factor
c_{var}	variable costs
$CO_{corr,e}$	correlation factor
$CO_{corr,p}$	correlation factor
CO_{CO_2}	cost of dispatch emission rights
$CO_{dispatch}$	dispatch regulation band costs
CO_{fuel}	variable fuel costs
$CO_{maintenance}$	variable maintenance costs
$CO_{start-up}$	dispatch start-up costs
$CO_{reduction}$	cost coefficient for reduced costs
dim	dimensionality of the latent space
e	energy supply gap
E	energy
\dot{E}	rate of charge
e_{epi}	auxiliary variable for energy supply gap
f	capacity factor
$f_{aemission}$	emission factor
f_{AN}	annuity factor
\mathbf{g}	vector of inequality constraints
h_{hub}	wind turbine hub height
\mathbf{h}	vector of equality constraints

i	interest
I	irradiance
\mathcal{I}	index set
\mathcal{K}	discretization set
$llpobj$	auxiliary variable for lower-level problem objective
\mathcal{L}	Lagrangian function
$mlpobj$	auxiliary variable for medial-level problem objective
\mathcal{N}	discretization set
n	number of a quantity
p	principal component
P	power
ppi	producer price index
pr	price
pr_{CO2L}	price for carbon dioxide emissions
pr_{fuel}	fuel price
$pr_{logistics}$	logistic costs
\mathcal{S}	set of representative scenarios
T	length of time horizon
t	time
\mathcal{T}	set of time steps
v_{wind}	wind speed
x_1	design variable for component 1
x_2	design variable for component 2
\mathbf{x}	vector of design variables
\mathcal{X}	feasible set of design variables
y	uncertain demand
\mathbf{y}	vector of uncertain variables
\mathcal{Y}	feasible set of uncertain variables
z	operational variable
z_0	roughness length

$z_{1,u}$	upper-level operational variable for component 1
$z_{1,l}$	lower-level operational variable for component 1
\mathbf{z}	vector of operational variables
\mathcal{Z}	feasible set of operational variables

Subscripts

<i>battery</i>	battery
<i>c</i>	component
<i>data</i>	data points
<i>days</i>	days
<i>demand</i>	demand
<i>diesel</i>	diesel
<i>dim</i>	dimension
<i>disc</i>	discretization
<i>e</i>	energy supply gap
<i>en</i>	energy system
<i>epi</i>	epigraph reformulation
<i>eq</i>	equations
<i>fix</i>	fixed
<i>hub</i>	hub height
<i>in</i>	input
<i>j</i>	index
<i>k</i>	index
<i>l</i>	index
<i>mon</i>	month
<i>nom</i>	nominal
<i>out</i>	output
<i>p</i>	principal components

<i>pca</i>	principal component analysis
<i>peak</i>	peak power
<i>ref</i>	reformulation
<i>s</i>	representative scenarios
<i>solar</i>	solar PV
<i>t</i>	time step
<i>therm</i>	thermal
<i>v</i>	vertices
<i>y</i>	upper level
<i>var</i>	variable
<i>wc</i>	worst-case
<i>wind</i>	wind turbine
<i>x</i>	design variables
<i>y</i>	uncertain variables
<i>yr</i>	year
z	operational variables
10m	10 meters

References

- Avis, D., Bremner, D., and Seidel, R. (1997). How good are convex hull algorithms? *Computational Geometry*, 7(5):265–301.
- Baumgärtner, N., Delorme, R., Hennen, M., and Bardow, A. (2019). Design of low-carbon utility systems: Exploiting time-dependent grid emissions for climate-friendly demand-side management. *Applied Energy*, 247:755–765.
- Davis, N. N., Badger, J., Hahmann, A. N., Hansen, B. O., Mortensen, N. G., Kelly, M., Larsén, X. G., Olsen, B. T., Floors, R., Lizcano, G., Casso, P., Lacave, O., Bosch, A., Bauwens, I., Knight, O. J., van Loon, A. P., Fox, R., Parvanyan, T., Hansen, S. B. K., Heathfield, D., Onninen, M., and Drummond, R. (2023). The Global Wind Atlas: A High-Resolution Dataset of Climatologies and Associated Web-Based Application. *Bulletin of the American Meteorological Society*, 104(8):E1507–E1525.

- Djelassi, H. (2020). *Diskretisierungsbasierte Algorithmen für die globale Lösung hierarchischer Optimierungsprobleme*. Dissertation, RWTH Aachen University.
- Enercon (2012). Enercon product overview. https://catalystresearch.wordpress.com/wp-content/uploads/2013/11/enercon_pu_en.pdf. Accessed: 2025-05-08.
- Euler, L. (2000). *Foundations of Differential Calculus*. Springer New York, New York, NY.
- European Commission (2022). JRC Photovoltaic Geographical Information System (PVGIS). https://re.jrc.ec.europa.eu/pvg_tools/en/. Accessed: 2024-11-12.
- eurostat (2024). Domestic Producer Prices Eurostat. <https://ec.europa.eu/eurostat/databrowser/bookmark/de68744b-c123-428d-a9c0-0f9cf843cdf7?lang=en>. Accessed: 2024-11-12.
- Figgenger, J., Hecht, C., Haberschusz, D., Bors, J., Spreuer, K. G., Kairies, K.-P., Stenzel, P., and Sauer, D. U. (2023). The development of battery storage systems in Germany: A market review (status 2023).
- Gobierno de Canarias (2023). Anuario Energetico De Canarias 2021. https://www.gobiernodecanarias.org/energia/descargas/SDE/Portal/Publicaciones/AnuarioEnergeticodeCanarias_2021_v2.pdf, Accessed: 2024-11-20.
- Gurobi Optimization, LLC (2024). Gurobi optimizer reference manual. <https://www.gurobi.com>.
- Hersbach, H., Bell, B., Berrisford, P., Hirahara, S., Horányi, A., Muñoz-Sabater, J., Nicolas, J., Peubey, C., Radu, R., Schepers, D., Simmons, A., Soci, C., Abdalla, S., Abellan, X., Balsamo, G., Bechtold, P., Biavati, G., Bidlot, J., Bonavita, M., De Chiara, G., Dahlgren, P., Dee, D., Diamantakis, M., Dragani, R., Flemming, J., Forbes, R., Fuentes, M., Geer, A., Haimberger, L., Healy, S., Hogan, R. J., Hólm, E., Janisková, M., Keeley, S., Laloyaux, P., Lopez, P., Lupu, C., Radnoti, G., de Rosnay, P., Rozum, I., Vamborg, F., Villaume, S., and Thépaut, J.-N. (2020). The ERA5 global reanalysis. *Quarterly Journal of the Royal Meteorological Society*, 146(730):1999–2049.
- Huld, T., Müller, R., and Gambardella, A. (2012). A new solar radiation database for estimating PV performance in Europe and Africa. *Solar Energy*, 86(6):1803–1815.
- Kost, C., Mayer, J. N., Thomsen, J., Hartmann, N., Senkpiel, C., Philipps, S., Nold, S., Lude, S., Saad, N., and Schlegl, T. (2021). Levelized Cost of Electricity Renewable Energy Technologies.
- MacQueen, J. et al. (1967). Some methods for classification and analysis of multivariate observations. In *Proceedings of the fifth Berkeley symposium on mathematical statistics and probability*, volume 1, pages 281–297. Oakland, CA, USA.

- Masters, G. M. (2004). *Renewable and Efficient Electric Power Systems*. Wiley, 1 edition.
- Ministerio de Industria, Energía y Turismo (2015). Real Decreto 738/2015, de 31 de julio, por el que se regula la actividad de producción de energía eléctrica y el procedimiento de despacho en los sistemas eléctricos de los territorios no peninsulares. <https://www.boe.es/buscar/act.php?id=B0E-A-2015-8646>. Accessed: 2024-11-20.
- Ministerio de la Presidencia (2006). Real Decreto 1370/2006, de 24 de noviembre, por el que se aprueba el Plan Nacional de Asignación de derechos de emisión de gases de efecto invernadero, 2008-2012. <https://www.boe.es/buscar/doc.php?id=B0E-A-2006-20530>. Accessed: 2024-11-20.
- Ministerio para la Transición Ecológica y el Reto Demográfico (2022). Orden TED/1315/2022, de 23 de diciembre, por la que en ejecución de la sentencia del Tribunal Supremo de 16 de noviembre de 2021, recaída en el recurso contencioso-administrativo 301/2020, se regulan las subastas para el suministro de combustible y determinación del precio de combustible, se autorizan nuevos combustibles, se establecen los valores unitarios de referencia, aplicable a las instalaciones de producción de energía eléctrica ubicadas en los territorios no peninsulares con régimen retributivo adicional, y se revisan otras cuestiones técnicas. <https://www.boe.es/buscar/doc.php?id=B0E-A-2022-23752>. Accessed: 2024-11-20.
- Ministerio para la Transición Ecológica y el Reto Demográfico (2023a). Resolución de 20 de junio de 2023, de la Dirección General de Política Energética y Minas, por la que se fija el poder calorífico inferior de la hulla, fuel oil, diesel oil, y gasoil para el primer y segundo semestre de 2022 a efectos del régimen retributivo adicional de los grupos de generación ubicados en los territorios no peninsulares. https://www.boe.es/diario_boe/txt.php?id=B0E-A-2023-14933. Accessed: 2024-11-20.
- Ministerio para la Transición Ecológica y el Reto Demográfico (2023b). Resolución de 21 de septiembre de 2023, de la Dirección General de Política Energética y Minas, por la que se fijan los precios de combustible en puerto aplicables al fuel oil, diesel oil, gasoil, y hulla en el primer semestre del año 2023 a aplicar en la liquidación de dicho período de los grupos generadores ubicados en los territorios no peninsulares. https://www.boe.es/diario_boe/txt.php?id=B0E-A-2023-20255. Accessed: 2024-11-20.
- Ministerio para la Transición Ecológica y el Reto Demográfico (2023c). Resolución de 5 de febrero de 2023, de la Dirección General de Política Energética y Minas, por la que se aprueba el precio de derechos de emisión de liquidación para el año 2022 en los sistemas eléctricos de los territorios no peninsulares. https://www.boe.es/diario_boe/txt.php?id=B0E-A-2023-4122. Accessed: 2024-11-20.

- Nahmmacher, P., Schmid, E., Hirth, L., and Knopf, B. (2016). Carpe diem: A novel approach to select representative days for long-term power system modeling. *Energy*, 112:430–442.
- Oke, T. R. (2006). *Boundary Layer Climates*. Routledge, London, 2nd ed edition.
- Pearson, K. (1901). On lines and planes of closest fit to systems of points in space. *The London, Edinburgh, and Dublin Philosophical Magazine and Journal of Science*, 2(11):559–572.
- Pedregosa, F., Varoquaux, G., Gramfort, A., Michel, V., Thirion, B., Grisel, O., Blondel, M., Prettenhofer, P., Weiss, R., Dubourg, V., Vanderplas, J., Passos, A., Cournapeau, D., Brucher, M., Perrot, M., and Duchesnay, E. (2011). Scikit-learn: Machine learning in Python. *Journal of Machine Learning Research*, 12:2825–2830.
- Pfeifroth, U., Kothe, S., Trentmann, J., Hollmann, R., Fuchs, P., Kaiser, J., and Werscheck, M. (2019). Surface Radiation Data Set - Heliosat (SARAH) - Edition 2.1. https://doi.org/10.5676/EUM_SAF_CM/SARAH/V002_01. Accessed: 2024-11-12.
- Red Eléctrica de España (2024). La Palma - Electricity demand tracking in real time. https://demanda.ree.es/visiona/canarias/la_palma5m/tablas. Accessed: 2024-11-12.
- Sass, S., Faulwasser, T., Hollermann, D. E., Kappatou, C. D., Sauer, D., Schütz, T., Shu, D. Y., Bardow, A., Gröll, L., Hagenmeyer, V., Müller, D., and Mitsos, A. (2020). Model compendium, data, and optimization benchmarks for sector-coupled energy systems. *Computers & Chemical Engineering*, 135:106760.
- Schubert, E. (2023). Stop using the elbow criterion for k-means and how to choose the number of clusters instead. *ACM SIGKDD Explorations Newsletter*, 25(1):36–42.
- Teichgraeber, H. and Brandt, A. R. (2019). Clustering methods to find representative periods for the optimization of energy systems: An initial framework and comparison. *Applied Energy*, 239:1283–1293.
- Thorndike, R. L. (1953). Who belongs in the family? *Psychometrika*, 18(4):267–276.
- Virtanen, P., Gommers, R., Oliphant, T. E., Haberland, M., Reddy, T., Cournapeau, D., Burovski, E., Peterson, P., Weckesser, W., Bright, J., van der Walt, S. J., Brett, M., Wilson, J., Millman, K. J., Mayorov, N., Nelson, A. R. J., Jones, E., Kern, R., Larson, E., Carey, C. J., Polat, İ., Feng, Y., Moore, E. W., VanderPlas, J., Laxalde, D., Perktold, J., Cimrman, R., Henriksen, I., Quintero, E. A., Harris, C. R., Archibald, A. M., Ribeiro, A. H., Pedregosa, F., and van Mulbregt, P. (2020). SciPy 1.0: Fundamental algorithms for scientific computing in Python. *Nature Methods*, 17(3):261–272.

- Zingler, A., Mitsos, A., Jungen, D., and Djelassi, H. (2023). libDIPS — Discretization-Based Semi-Infinite and Bilevel Programming Solvers. *Optimization Online*, 24914.